Epitaxial growth of p-type doped III-V nitride semiconductor on sapphire substrate using remote plasma metal organic chemical vapor deposition

Chandana Rangaswamy

Presented to the faculty of Electrical and Computer Engineering in fulfillment for a M.Sc. degree

Lakehead University
Thunder Bay, Ontario
August 2019

Table of contents

Chapter 1. Introduction……………… ……………………………1
1.1 III-V nitride overview……………. ……………………………2
1.2 Gallium nitride background………………………………………3
1.3 Substrates for Gallium Nitride……………………………………4
Chapter 2. Precursors…………………… ………………………5
2.1 PRECURSORS OF THE GROUP III…………………………….6
2.2 TMGa and TEGa………………………………………………….7
2.3 DEGaCl……………………………………………………….13
2.4 Nitrogen precursor…………………… ………………………15
2.5 P-dopant precursor………………………… …………………16
Chapter 3: Group III-Nitride Growth technology………………………18
3.1 Two stage growth process…………………………………….18
3.2 Growth Technology…………………………………………..19
3.2.1 Nitridation…………………………………………………..20
3.2.2 ALD………….. ……………………………………………...20
3.2.3 HVPE………………… …………………………………......21
3.2.4 Physical vapour Deposition….. …………………………..…..22
3.2.4.1 MBE…………………………………………………..…..22
3.2.5 MOCVD…………………………………….………………....25
3.2.6 Plasma Assisted Growth technique……………………………26

3.2.7 Lakehead reactor……………………………………………..29

Chapter 4: Characterization techniques…………………………….34
4.1 X-Ray Diffraction……………………………………………34
4.1.1 Measurement Technique…………………………………...38
4.2 Scanning Electron Microscope……………………………….38
4.2.1 Measurement Technique…………………………………...40
4.3 Energy-dispersive X-ray Spectroscopy…………………….…41
4.4 Atomic Force Microscopy…………………………….………42
4.4.1 Measurement Technique……………………………………43
4.5 Hall Effect………………………………………………………45
4.5.1 Measurement technique………………………………………46
4.6 X-ray Photoelectron Spectroscopy (XPS) ………………………48

Chapter 5: Difficulties of Mg-Doped GaN……………………………..49
5.1 Solubility…..…………………………………………………….49
5.2 Surface segregation and pyramidal defects………………….….51
5.3 Memory effect…………………………..……………………….55
5.4 High vapor pressure…………………………………………..….57
5.5 Low sticking coefficient………………………………………….59
5.6 High ionization energy…………………………..……………61
5.7 Unintentional dopants………………………………….………..63
5.8 Compensating defects……………………………………………..64

Chapter 6: Growth and Result……………………………….…………….……………67
6.1 Growth Preparation…………………..…………………………………………68
6.2 Results for p-doped GaN…...………………………………………………69
Chapter 7: Conclusion and Reference…..…...……………………………….78

List of figures

Figure.1: Bowing of the Ternary Alloys of the Group III-Nitrides [73].

Figure 2: Decomposition of TEGa and TMGa as a function of temperature by different carrier gas [25].

Figure.3: AFM surface images for GaN epilayers grown with (a) TMGa and (b) TEGa [26].

Figure.4: In site normal reflectance measure of the entire sequence of GaN growth as a function of growth time (a) GaN with TMGa (b) GaN with TEGa [30].

Figure.5: Typical AFM images of the GaN surface morphology [40].

Figure.6: (a) Comparison of the I-V characteristics for the only Mg-doped (dashed line) and Mg-Zn co-doped p-type GaN films (solid line), (b) Variation of resistance as a function of gap spacing for the only Mg-doped (Solid square) and Mg-Zn co-doped (solid circle) p-type GaN films [52].

Figure.7: The discovery of high quality GaN growth techniques in 1986 led to their development as a key research material [55].

Figure.8: Thermal decomposition efficiency of ammonia. The sudden onset of cracking efficiency sets a lower limit on temperature in nitride growths [59].

Figure.9: Typical MBE deposition chamber [60].

Figure.10: Possible effects of high energy ions on ALD growths. These effects are not specific to ALD and directly apply to both MBE and MOCVD techniques [73].

Figure.11: The gas cabinet of the Lakehead experimental reactor. This cabinet controls all gas flow to main chamber through pneumatic valves and maintains temperatures vapour flow in the lines [63].

Figure.12: Lakehead University Remote Plasma-Enhanced MOCVD System.

Figure.13: X-ray diffraction schematic (a) illustration of the conditions required for Bragg diffraction to occur and (b) relationship of the incident (k0), diffracted (kh) and scattering (S) vectors with respect to the crystal. Planes of atoms are indicated by dotted lines; these are not necessarily parallel to the sample surface [66].

Figure.14: A section through reciprocal space for an [0001]-oriented GaN film. Regions of reciprocal space where the sample blocks a beam are shown in grey (inaccessible). The vectors k_0 and k_h have the length $1/\lambda$ (where λ = 1.54 Å); the vector S has a length of $1/d$ [0004] and is

perpendicular to the [0004] plane. The Ewald sphere is shown here as a circle, cutting the [0004] reciprocal lattice spot. Some spots are absent as they have an intensity of zero [67].

Figure 15: Schematic of a typical SEM beam and electron gun [68].

Figure 16: Interaction bloom in a sample caused by the interacting electrons [69].

Figure 17: Schematic on how an electron is removed from the K-Shell [70].

Figure.18: Schematic of typical AFM [71].

Figure.19: Schematic drawing of Hall measurement [107].

Figure 20: Cross section view of defects on top and surface view of defects on bottom [85].

Figure.21: Response of defect-free thickness to precursor ratio, showing complete defect free growth for a molar precursor ratio less than 0.02 [85].

Figure.22: Relationship of defect density and thickness, showing an initial defect-free offset and following oscillation with period [85].

Figure.23: (a) Demonstrated memory effect of Mg-doped GaN, with (b) interruption solution showing no delay in Mg incorporation [88].

Figure.24: Vapor pressure curve for Mg which shows a steep slope for low temperature, which are used for dopant-level fluxes [92].

Figure 25: Energy diagram of GaN showing energy levels of donors and acceptors and the thermal energy at room temperature [97].

Figure 25: Formation energy as a function of Fermi level for Mg in different configurations (Ga-substitutional, N-substitutional and interstitial configuration). Vacancies and interstitial H are also included [107].

Figure 26: Combined XRD results of samples.

Figure 27: Cross sectional view of SEM result of sample 4.

Figure 28: Cross sectional view of SEM result of sample 4 with film thickness measurement.

Figure 29: EDX result of sample 4 spectrum 1.

Figure 30: EDX result of sample 4 spectrum 2.

Figure 31: Cross sectional view of SEM result of sample 5.

Figure 32: Cross sectional view of SEM result of sample 5 with film thickness measurement.

Figure 33: EDX result of sample 5 spectrum 1.

Figure 34: EDX result of sample 5 spectrum 2.

Figure 35: XPS result of sample 8.

Figure 36: The photoluminescence spectra of Mg-doped GaN (a) with microwave treatment (b) with thermal annealing (c) as grown without any treatment [112].

Figure 37: Resistivity of Mg-doped GaN with different microwave treatment time [112].
.
Figure 38: The carrier concentration of Mg-doped GaN by Hall measurement with different microwave treatment time [112].

List of Acronyms

Metal Organic Chemical Vapour Deposition (MOCVD)

Remote Plasma Metal Organic Chemical Vapour Deposition (RP-MOCVD)

Gallium Nitride (GaN)

Light Emitting Diode (LED)

Molecular Beam Epitaxy (MBE)

Atomic Layer Deposition (ALD)

Full Width at Half Maximum (FWHM)

Residual Gas Analyzer (RGA)

Metal Organic (MO)

Atmospheric Pressure- Metal Organic Chemical Vapour Deposition (AP-MOCVD)

Low Pressure- Metal Organic Vapour Deposition (LP-MOCVD)

Secondary Ion Mass Spectroscopy (SIMS)

Acknowledgement

I would like to thank my supervisor Dr.Dimiter Alexandrov for his support in the research performed for my thesis. The technical support received from him during the growth and characterizing grown sample was extremely useful.

I like to thank my lab colleague who worked with me in the Lakehead University semiconductor laboratory. They helped me identify my thesis topic, showed how to operate the lab equipment, clarified all my doubts regarding the subject.

I would like to thank my family who supported through out my journey with lots of encouragement.

Abstract

Lakehead University Remote Plasma-enhanced Metal Organic Chemical Vapour Deposition (RP-MOCVD) is used to grow III-V nitride semiconductor material. RP-MOCVD use nitrogen plasma as a nitrogen source along with group III precursor for epitaxial growth of III-V nitride. Using plasma for the growth process is advantages over conventional MOCVD as it uses ammonia for nitrogen source. As ammonia dissociate at higher temperature, restrict the growth for certain material thus limiting the selection of substrate for the growth process. RP-MOCVD is efficient as it operates at low temperature and uses plasma for growth.

In this work p-type acceptor doped GaN epitaxial growth using RP-MOCVD is discussed. Mg is used as a dopant element to obtain p-type in GaN. Achieving p-type doping always remains a difficult issue for electronic and optical devices. Mg doped GaN has hole concentration around $1x10^{18}$ cm^{-3} due to saturation in p-type conductivity when Mg concentration is increased. Polarity of GaN matter during the growth, with Ga-polar GaN the hole concentration is higher compared with N-polar GaN. Temperature is one of the main factor in RP-MOCVD determining

p-type conductivity in GaN film which provide room for compensation effect, solubility issue and dopant incorporation.

The growth result obtained from RP-MOCVD are analysed using X-ray diffraction (XRD), Scanning electron microscopy (SEM), Atomic force microscope (AFM), Hall effect, X-ray photoelectron spectroscopy (XPS).

Chapter 1. Introduction

III-V nitride semiconductors were first synthesized in 1928 by many growth techniques. Molecular Beam Epitaxy (MBE), Hydride Vapor Phase Epitaxy (HVPE), Metal Organic Chemical Vapor Deposition (MOCVD) are the growth techniques used to obtain III-V nitrides. Usually GaN growth is n-type due to nitrogen vacancies but later it was concluded n-type nature of grown GaN is due to oxygen impurity incorporated during the growth. In the late 1980's first p-type doping in GaN using Mg doping was achieved using low energy electron beam irradiation [1,2]. N-type and p-type III-V nitride semiconductor carrier concentration with low resistivity are required for optoelectronic device applications. Doping GaN to obtain n-type semiconductor is easy compared to obtaining p-type GaN. GaN is doped with either group II elements such as Be, Mg, Ca, Zn and Cd or group IV elements such as C, Si and Ge to obtain p-type growth film. Zn was the first element used for p-type doping in GaN but resulted in semi-insulating material due to large activation energy, thus making the material highly resistive [3-5]. Cd was used to dope GaN sample but failed to over come electron background concentration [6]. When carbon is used for p-type doping in GaN its difficult to achieve the required result as it takes both N and Ga lattice site [7]. Si has been used to obtain p-type doping but instead of p-type dopant it resulted in n-type in GaN film. Mg has been reported a successful element to obtain p-type doing in GaN using MOCVD or MBE. Post

growth treatment is required to increase hole concentration in GaN. Mg used to dope GaN is passivated by hydrogen by forming Mg-H complexes. Amano et al. used post growth treatment, low energy electron beam irradiation to activate Mg acceptors in GaN film [8]. Post growth thermal annealing treatment is effective to activate Mg acceptors when GaN film is grown by MOCVD [9]. Activation energy of Mg is 250meV which is very large thus at room temperature leading to low acceptor activation [10]. Theoretically, as Ca does not have d-electrons, it is superior to Mg for obtaining p-type doping in GaN [11]. Activation energy of Be is approximately 98meV [12,13] suggest as a shallowest p-type dopant but Be atom is too small and incorporate interstitial site acting as double donor.

1.1 III-V nitride overview

Group III-V nitride semiconductor are main interest because they have direct bandgap 0.69eV to 1.89eV for InN, 3.4eV for GaN and 6.2eV for AlN [14]. For ternary alloys each of these three can be combined in different concentration. Due to this alloying, it is easy to tune ternary alloys optical absorption edge to any required optical absorption edge along the lines as shown in figure.1. Crystal structure are of three form that is rock salt, wurtzite, zinc blende among them wurtzite is the most stable one.

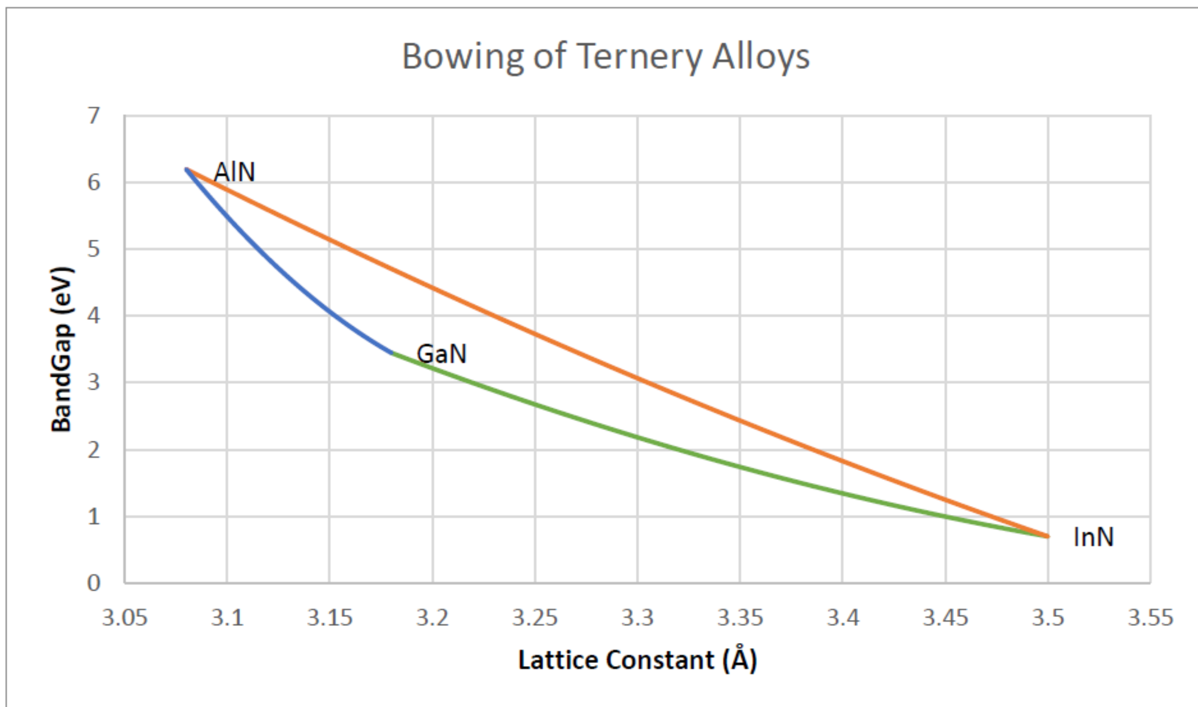

Figure.1: Bowing of the Ternary Alloys of the Group III-Nitrides [73]

1.2 Gallium nitride background

Gallium nitride has wide band gap, high temperature tolerance and conductivity, can tolerate very high electric field (handing both high voltage and high current). Break down field of GaN is $5X10^6$ V/cm allowing reverse blocking capability to greater extent. Reverse breakdown is through either Zener effect or avalanche effect. Zener effect is more difficult due to GaN large band gap. Electron mobility of GaN is $1500cm^2/V*s$. GaN photodiodes are used for detecting ultraviolet or blue region radiation from visible spectrum.

1.3 Substrates for Gallium Nitride

Deposition of gallium nitride is usually done using one of the three substrates sapphire, silicon [111] or silicon carbide (4H or 6H). Due to crystal quality and price, sapphire is most commonly used substrate. Lattice mismatch with GaN is fairly large (16.1%) when sapphire is the substrate used for the growth and a good thermal conductivity for high power handing. GaN doped with magnesium atoms to obtain p-type doping, the doped impurity exert compressive force on the GaN film. This force mitigates mismatch strain by matching substrate with the film. Sapphire substrate used for III-V nitride growth is typically used in lasers, UV and blue or violet LED and high frequency transistors.

When Si [111] is used to grow GaN, the mismatch (17%) give rise to tensile force on GaN, doped acceptor impurity used for doping. When Si is used as a substrate to grow, GaN buffer layer is required to achieve good growth.

Silicon carbide lattice mismatch with GaN is 3.5% which is very less compared to sapphire or silicon. But the main draw back with silicon carbide is very expensive thus restricting its use for the growth.

Chapter 2. Precursors

The growth of III-nitride thin films significantly influenced by selection of precursors. The precursor used for the growth of group III-nitride, n-doping and p-doping are presented and their characteristic are discussed. Some precursors have very distinctive effects on sample properties when used during the growth, such as TMGa and TEGa, these precursors are compared in detail.

Precursors are source materials for each element such as Al, Ga, In, N, Si, Mg and so on. Depending on the growth condition they are in solid, liquid or gas state. There is a huge investigation of metalorganic precursors for the growth of semiconductor [15]. After enormous research on fundamental properties of an ideal precursors, the properties of precursors can be defined as (1) precursors should have a good volatility (preferably higher than 0.1 torr at around 300k) (2) have a good thermal stability during the time of its evaporation and transport in the gas phase (3) without contamination of the growing film precursors must decompose cleanly on pyrolysis. Along with these three main properties, it should have high purity, non-pyrophoric and be non-toxic. Also, should be stable in a container for a longer period as it is often used in a limited amount. liquid precursors are better than a solid and gaseous, as it provides stable vapor pressure. Table.1 provides a common chemical precursors for the growth and doping of III-nitride.

Element	Chemical formula	Chemical name	Pressure(298K)	Melt point(^oC)	Toxicity
Ga	$(CH_3)_3Ga$	TMGa	238	-15.8	Pyrophoric
	$(C_2H_5)_3Ga$	TEGa	4.79	-82.5	Pyrophoric
Al	$(CH_3)_3Al$	TMAl	14.2	15	Pyrophoric
	$(C_2H_5)_3Al$	TEAl	0.041	-52.5	Pyrophoric
In	$(CH_3)_3In$	TMIn	1.75	88	Pyrophoric
	$(C_2H_5)_3In$	TEIn	0.31	-32	Pyrophoric
Zn	$Zn(C_2H_5)_2$	DEZn	8.53	-28	Pyrophoric
Mg	$Mg(C_5H_5)_2$	Cp_2Mg	0.05	175	Pyrophoric

Table.1 The most common chemical precursors for the growth and doping of III-nitride [106]

2.1 PRECURSORS OF THE GROUP III

For the growth of group III-V nitrides there are several metal organic compounds used as precursor shown in the table.1. In these available precursors, trimethyl compounds and triethyl compounds are most frequently used. Trimethyl compounds react more easily at the atmospheric reactors as they have higher vapor pressure than that of trimethyl compounds.

Along with low vapor pressure, triethyl compounds undergoes severe parasitic reaction thus making them not suitable for the atmospheric pressure (AP) growth [16]. It has been noted that the pre-reaction between the precursors might leads to the formation of stable Lewis acid-base adducts and oligomers with continuous elimination of hydrocarbons [17-19]. Trimethyl compounds can react with NH_3 given an atmospheric pressure (AP) circumstance. TMGa produces stable cyclic trimers $[(CH_3)_2GaNH_2]_3$[17] and TMAl undergoes parasitic pre-reaction which can severely impact on the quality if the film deposited in the AP-MOCVD reactors. To grow high purity GaN with less carbon contamination at low pressure reactors triethyl compounds have been used [20]. It has also been observed that decomposition of triethylaluminium, - gallium, -indium take place at lower growth temperature compared with trimethyl equivalents [21], and thus at low temperature higher Ga/Al/In contents in gas phase can be achieved.

2.2 TMGa and TEGa

Compared with aluminum precursor, the selection of gallium precursors has greater impact to the films deposited [22]. For the growth of gallium nitride the most frequently used precursor are TMGa and TEGa. TEGa is only suitable to the LP-MOCVD while TMGa is suitable to both LP-MOCVD and AP-MOCVD. But the use of TEGa to the LP-MOCVD has series of advantages [23]. TEGa has a lower decomposition temperature as seen in figure.2 and can be easily applied to the low temperature

condition. The growth of GaN by TMGa and TEGa has different kinetic model. When TMGa is used for the growth it undergoes two reaction 2.2a and 2.2b.

$$Ga(CH_3)_3 \rightarrow Ga(CH_3)_2 + CH_3 \quad (2.2a)$$

$$Ga(CH_3)_2 \rightarrow GaCH_3 + CH_3 \quad (2.2b)$$

Homogeneous decomposition of TMGa take place in reaction 2.2a with the loss of a methyl radical resulting in dimethyl-gallium (DMGa). Further resulted DMGa decompose to monomethyl-gallium (MMGa) by loss of another methyl radical. MMGa is highly mobile molecule with long diffusion length acting as the determining species at the substrate [24].

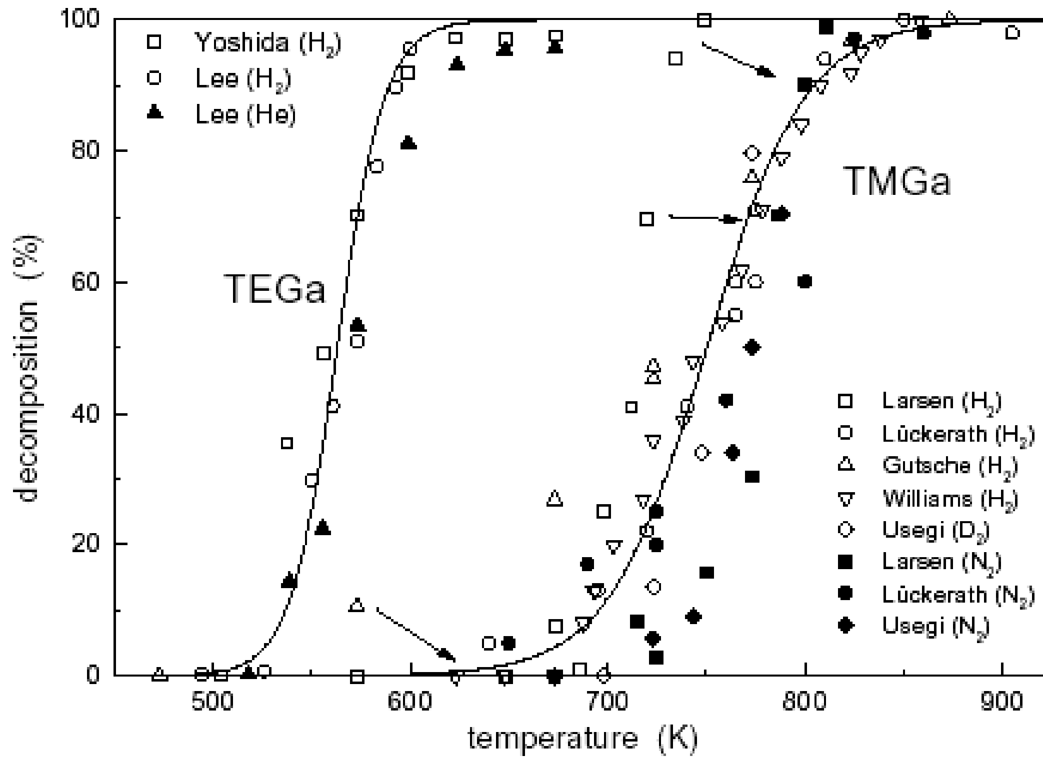

Figure 2: Decomposition of TEGa and TMGa as a function of temperature by different carrier gas [25]

On the other hand, with TEGa the decomposition takes place by elimination [26].

$$(CH_3 - CH_2) - Ga - R \rightarrow CH_2 = CH_2 + H - Ga - R \qquad (2.2c)$$

Highly reactive gallane (GaH_3) molecule can be obtained as the activation energy for this decomposition is low. This gallane molecule acts as the growth determining species of TEGa. Due to very small diffusion length gallium can incorporate easily into the crystal near to the place where it arrives on the surface. Figure.3 shows AFM surface image of GaN epitaxy

grown with identical conditions except gallium precursors. The surface morphology of the GaN film grown with two precursors are different. The root mean square surface roughness of AFM sample grown by TEGa is 16.4Å while by TMGa is 9.59Å. The reason for this difference is due to the different diffusion length.

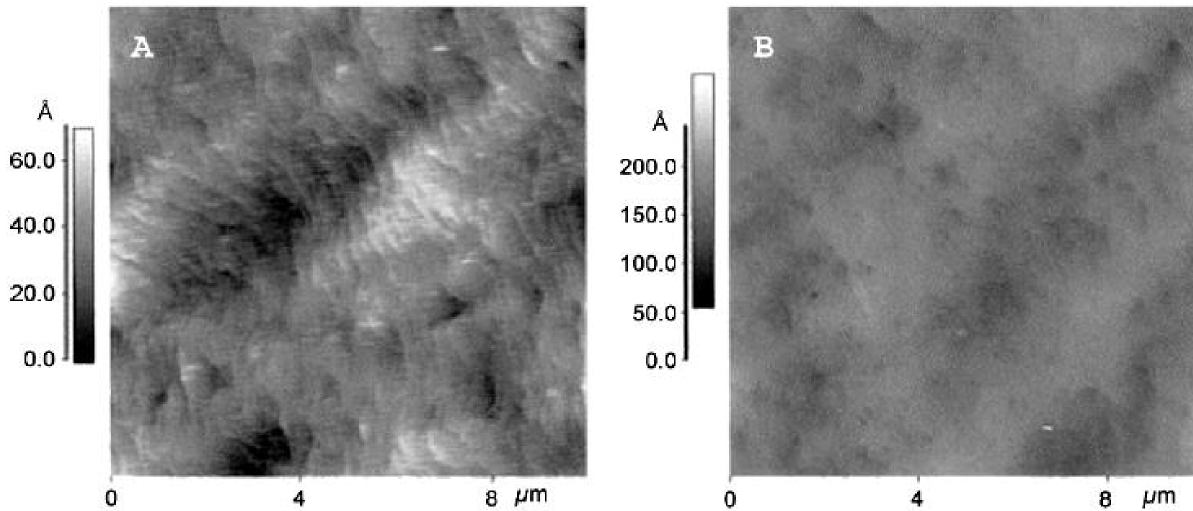

Figure.3: AFM surface images for GaN epilayers grown with (a) TMGa and (b) TEGa [26]

The lateral growth is restricted due to small diffusion length of GaH_3 where Ga atom is stick to the place where it arrives the surface thus resulting in rough surface. Using TEGa as Ga precursor instead of TMGa can reduce carbon contamination during the GaAs [27] or InGaAs [28] growth. The same conclusion can be drawn for GaN growth [29,30]. The

reduction in carbon provide different mechanism: H and C contamination in GaN growth can be introduced by highly reactive methyl group compared with steady C_2H_4. Often carbon contamination makes GaN film highly resistive by compensating native defects or residual impurity such as Si and O.

The crystallinity of GaN can be improved by the reduction of impurity. The FWHM from XRD of sample with TMGa is higher compared with TEGa as shown in table 2. The in site normal reflectance measurement has been done on the growth of TMGa and TEGa as shown in figure 4. The island coalescence stage (impact on the quality of GaN differ from the growth process with TMGa and TEGa. The coalescence stage in the case of TMGa is much shorter indicating the growth mode changing from three dimensional to quasi-two dimensional but with TEGa such a period goes for longer time, gradually coalescence procedure take place and gradually the growth mode is changed.

Value (arcmin)	Category	Sample with TMGa	Sample with TEGa	Priority of sample with TEGa
FWHM of [002] Teta-rocking	Symmetric curves	9.982	8.043	Less screw dislocation and mixed dislocation
FWHM of [102] Teta-rocking	Asymmetric curves	11.472	10.970	Less threading dislocation
FWHM of [102] hk-circle scan	Angular rotation of columns	16.806	15.306	Neighboring columns are aligned better

Table.2: The result of X-ray rocking for GaN films [36]

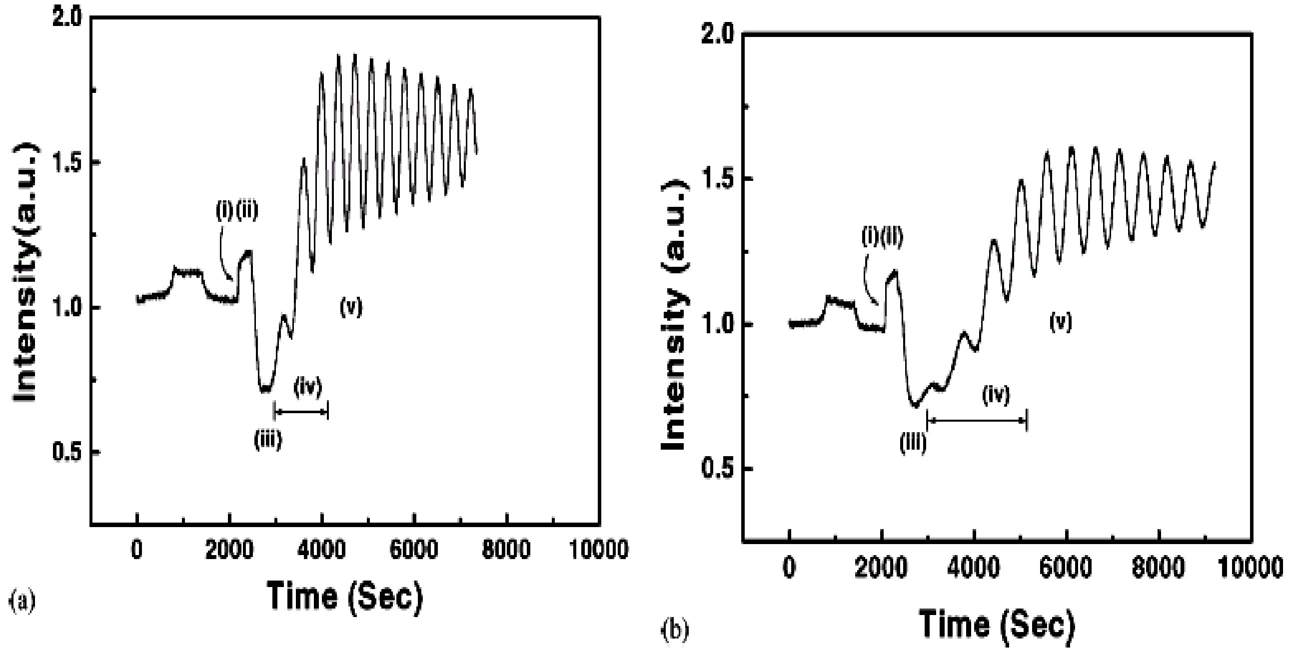

Figure.4: In site normal reflectance measure of the entire sequence of GaN growth as a function of growth time (a) GaN with TMGa (b) GaN with TEGa [30]

2.3 DEGaCl

The alternative precursor for gallium is DEGaCl ($(C_2H_5)_2GaCl$) [37-40]. To achieve hydride vapor phase epitaxy (HVPE) this precursor is used resulting in high quality growth and less carbon contamination with GaAs growth thus being advantage with MOCVD [39]. DEGaCl decompose as beta- elimination reaction (2.2c) forming GaCl [40]. 2.3a and 2.3b is the reversible reaction that take place in MOCVD.

$GaCl_3 + NH_3 \rightarrow GaN + H_2 + HCl$ (2.3a)

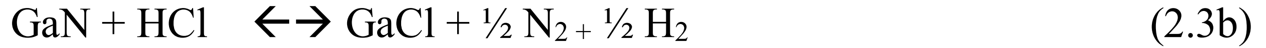

$$GaN + HCl \leftrightarrow GaCl + \frac{1}{2} N_2 + \frac{1}{2} H_2 \quad (2.3b)$$

HCL is believed to improve surface structure and removal of chemical defects and impurities. Surface morphology of a sample grown with TMGa and DEGaCl are different. There is sharp faceted step edge surface morphology with the sample grown with DEGaCl which is similar to the sample grown with HVPE as shown in figure 5

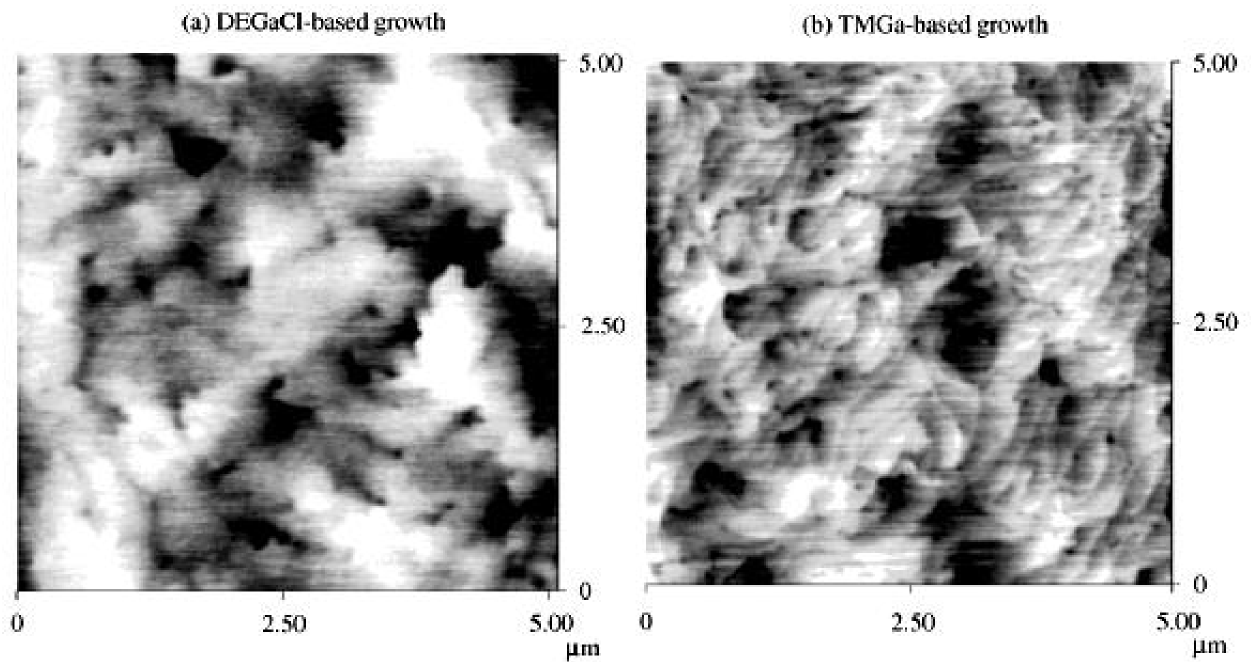

Figure.5: Typical AFM images of the GaN surface morphology [40]

2.4 Nitrogen precursor

For MOCVD the most common nitrogen precursor is ammonia for the growth of III-V nitrides. High stability of ammonia is achieved when epitaxial growth is carried at higher temperature. Sometime high temperature growth causes issues for example InN growth is difficult to achieve at higher temperature due to low decomposition thus prefer low temperature growth. There are potential precursor source available for nitrogen these include Dimethylhydrazine ($(CH_3)_2NNH_2$), triethylamine ($(C_2H_5)_3NH_2$), phenylhydrazine ($(C_6H_5)NHNH_2$), $N(CH_3)_3$), t-butylamine ($(C_4H_9)_3CNH_2$) and tertiarybutylamine ($N(C_4H_9)H_2$). With the use of $N(CH_3)_3$ the growth result did not show any GaN epitaxial layer instead Ga droplets [41]. Low III/V ratio limit the growth for both triethylamine and t-butylamine. There is carbon deposit in the case of t-butylamine which is intrinsic limitation [42] also tertiarybutylamine is associated with high level of carbon incorporation during the growth of GaN and AlN [42]. Temperature reduction during the deposition has been observed with the use of phenylhydrazine because of low thermal stability [43]. The promising alternative for NH_3 is dimethylhydrazine ($(CH_3)_2NNH_2$), due to it lower thermal stability there is reduction in deposition temperature and nitrogen flux is available sufficiently because of good volatility. It has been reported that high quality GaN growth has been achieved using this

precursor [44.45]. Among all these precursors ammonia has been widely used precursor for nitrogen in MOCVD for the growth of III-V nitride.

2.5 P-dopant precursor

P-type acceptor impurity doping in III-V nitride are achieved from group III elements. Among group III elements Mg is the most promising species for obtaining p-type doping in III-V nitride semiconductor growth in MOCVD [46,47]. Bis-cyclopentadienyl magnesium (Cp_2Mg) is the precursor used for obtaining p-type doping in III-V nitride. Cp_2Mg is a solid material with a low volatility (0.04 torr at 300k), to achieve gas phase heating above room temperature is required [48]. Bismethylcyclopentadienyl magnesium ($(MeCp)_2Mg$) and bisethylcyclopentadienyl magnesium (ECp_2Mg) are considered as a alternative for Cp_2Mg, they have lower melting point and higher vapour pressure. To fabricate high quality device this precursor is used [49]. Post growth treatment is required to achieve high acceptor concentration, hole concentration in the range 10^{18} cm^{-3} is obtained with post growth thermal annealing at the temperature 750°C in N_2 ambient [50]. The presence of methyl group is believed to strongly affect interaction with NH_3 thus increases precipitate formation in the growth chamber or at the surface.

ECp_2Mg is liquid at room temperature thus providing stable vapor pressure when compared with Cp_2Mg. After post growth thermal annealing treatment on GaN films, shows p-type conduction [51]. Post

growth treatment such as low energy electron beam irradiation or thermal annealing above 600°C under nitrogen or vacuum is required to break Mg-H bonds and activate acceptor impurity [52,53]. The activation energy of Cp_2Mg is bit higher than ECp_2Mg that is 170meV for Cp_2Mg [54] and 163meV for ECp_2Mg [51]. Zn can be used as an alternative species for p type doping. Diethyozinc (DEZn) is the precursor source for co-doping showing a low electrical resistivity (0.7 Â cm) and high hole concentration up to 8.5×10^{17} cm^{-3} without any loss of quality of the sample [52]. The specific contact resistance is one order of magnitude lowered by using Mg-Zn co-doping as shown in figure.6.

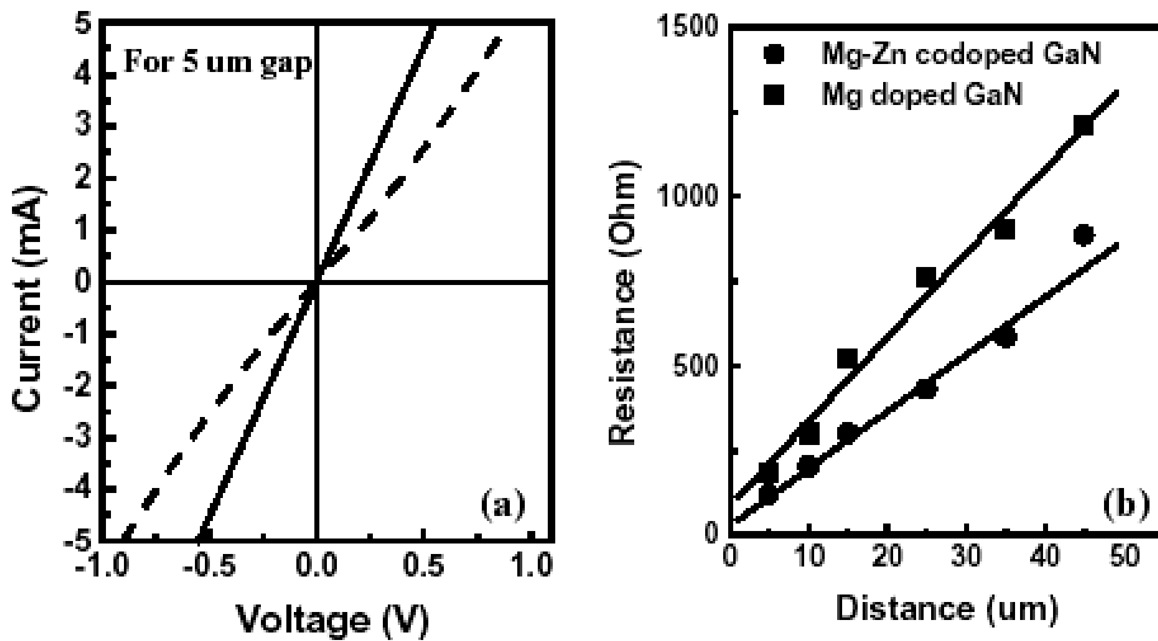

Figure.6: (a) Comparison of the I-V characteristics for the only Mg-doped (dashed line) and Mg-Zn co-doped p-type GaN films (solid line), (b) Variation of resistance as a function of gap spacing for the only Mg-doped (Solid square) and Mg-Zn co-doped (solid circle) p-type GaN films [52]

Chapter 3: Group III-nitride growth technology

In this chapter the growth technology used for III-V nitride is described. This chapter provides the practical implementation of growth process by providing operational principles, different growth techniques used for growth of III-V nitrides and the limitation involved in the growth process.

3.1 Two stage growth process

Two stage growth process is the first growth process used to grow III-V nitrides in 1986 by H.Amano et al[53] where a thin layer of AlN at low temperature is grown on sapphire substrate, later GaN at higher temperature is grown around 950-1060°C. The growth result obtained from this technique was very smooth which let to the further investigation in the field of III-V nitride semiconductor. Figure.7 shows the research done in the years in the nitride semiconductor field. This research let to the growth of GaN with buffer layers to get a better result also growing p-type GaN using Mg precursor [54]. It has been observed that using buffer layers during the growth process helps to minimise defect in the film and mismatch between substrate and layers to be deposited.

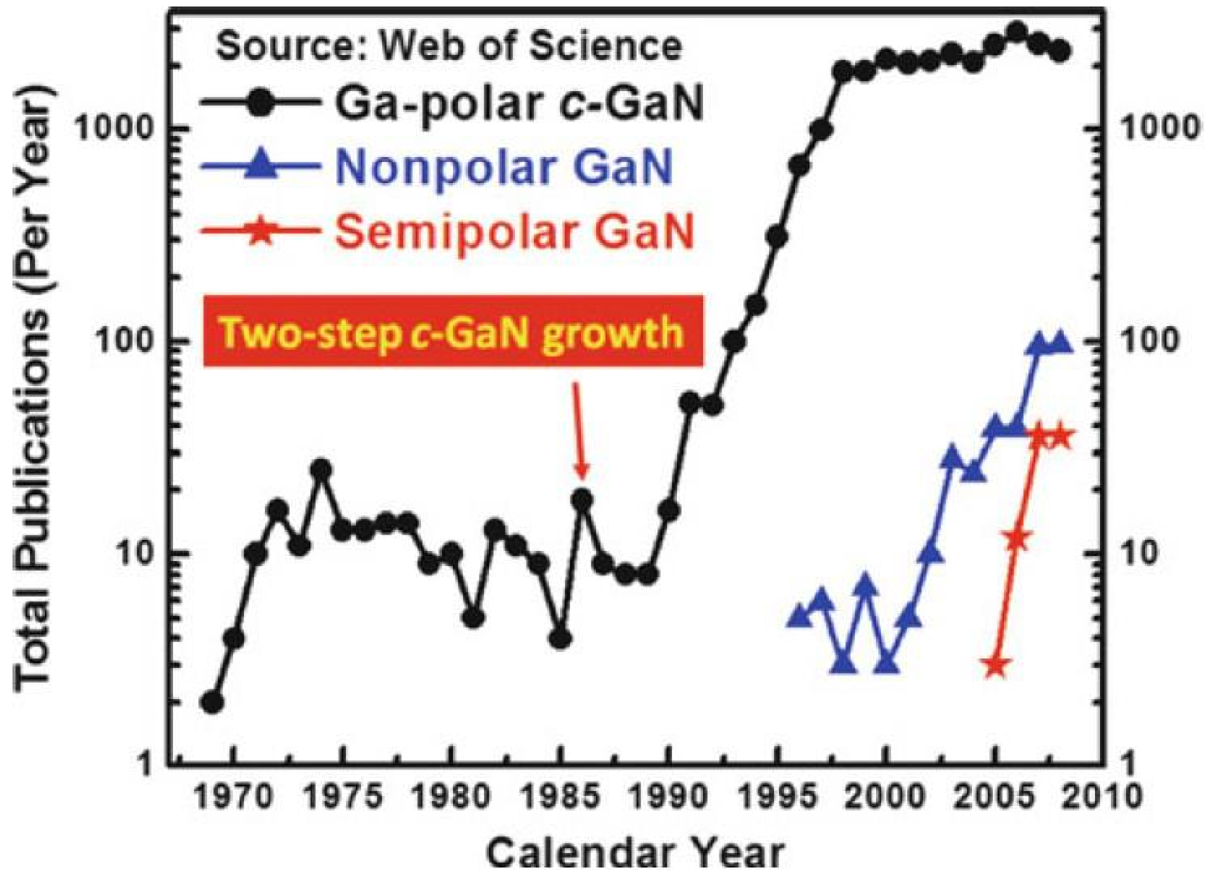

Figure.7: The discovery of high quality GaN growth techniques in 1986 led to their development as a key research material [55].

3.2 Growth Technology

There are variety of growth techniques used to grow III-V nitride semiconductors. Each growth technique has its advantage and disadvantage. Following section describe operational technique used in each method and the technique used for the growth of p-type doped GaN.

3.2.1 Nitridation

Nitridation is a process of exposing a film sample used for the growth process to nitrogen [56]. Nitridation helps in improving electrical and optical properties of the sample along with surface morphology in low temperature growth [57].

3.2.2 ALD

Atomic layer deposition (ALD) is a process that involves sequential self limiting half reactions cycle in loops to provide high quality film growth. Due to surface saturation during each half cycle, high conformity and uniformity is achieved. There is less impact on the deposition with respect to reactants, substrate and temperature when sufficient time is provided for saturation. To minimize unwanted vapour phase reaction, surface controlled growth needs in-between purging of the chamber half reaction. The growth of GaN through ALD undergoes following steps. First TMGa is introduced into the chamber. This TMGa is absorbed chemically by nitrogen due to previous nitrogen surface treatment thus leaving behind $(CH_3)_2Ga$ attached to the surface. Inert gas is used to remove gaseous by-product reaction and non-reacted precursor. Nitrogen in the form of nitrogen plasma or ammonia is introduced in the chamber. The decomposed nitrogen from ammonia or nitrogen plasma reacts with $(CH_3)_2Ga$ by taking remaining methyl ligands. For the next TMGa step the nitrogen atom is left in each surface with dangling bond. The final step

involves removal of unwanted or unreacted gas that is purging. The disadvantage in this technique is attaining surface saturation and extra purging step which result in limited growth rate.

3.2.3 HVPE

Hydride Vapour Phase Epitaxy (HVPE) technique use HCL vapour to react with liquid source element or solid source element. HVPE is a chemical vapour deposition (CVD) uses HCL vapour thus transporting III-chloride vapour to substrate chamber. The first step in HVPE for GaN growth can be given as shown below:

$$2HCl + 2Ga => 2GaCl_2 + H_2 \quad (3.2.3a)$$

For group V source, hydride vapours such as ASH, PH and NH is used. The growth reaction for GaN inside the chamber is show below

$$GaCl + NH_3 + H_2 => HCl + 2H_2 \quad (3.2.3b)$$

The advantage of HVPE growth is elimination of carbon contamination in the chamber but the by-product of HCL maybe an issue for the growth process. The growth of thin film for quantum well and super lattice structure using HVPE is certainly difficult. Though HVPE is not preferred for modern device layer growth, it is used for non-polar oriented growth of GaN [58]

3.2.4 Physical vapour Deposition

Physical vapour deposition (PVD) is a thin film deposition method under vacuum. The gas required for the growth are produced by sputtering, evaporation or a non-chemical based method. Generally, material required for the deposition is either in solid state or evaporated into the atomic species. This growth method overcome atomic binding energy by transferring kinetic energy [58]. Usually plasma is used during growth process in this method. The common PVD is molecular beam epitaxy (MBE)

3.2.4.1 MBE

Molecular Beam Epitaxy (MBE) is a thin layer deposition method which uses ultra high vacuum (UHV). Through thermal evaporation of elemental sources in the effusion cells molecular beams are formed under high vacuum. The evaporated elements in the growth chamber have long mean free paths due to high vacuum system compared with chamber dimensions because of this a beam like path in vapour phase is generated by neglecting all parasitic gas reactions of elemental vapours which is high purity layer. By the geometry and temperature of the system the beam trajectory and flow rate are maintained. The effusion cell mainly holds a crucible, cooling element for thermal isolation, heating element and a mechanical shudder. No precursor of chemical reaction is required as MBE uses elemental precursors. This method used for growth is

advantageous as contamination like carbon and oxygen can be eliminated compared with CVD process. Growth of III-V nitride semiconductor by MBE can utilize ammonia for nitrogen source but when ammonia is used as nitrogen source the temperature of growth must be above 600°C as shown in the figure.8. Unwanted defects and stress can be introduced during the growth process due to thermal expansion.

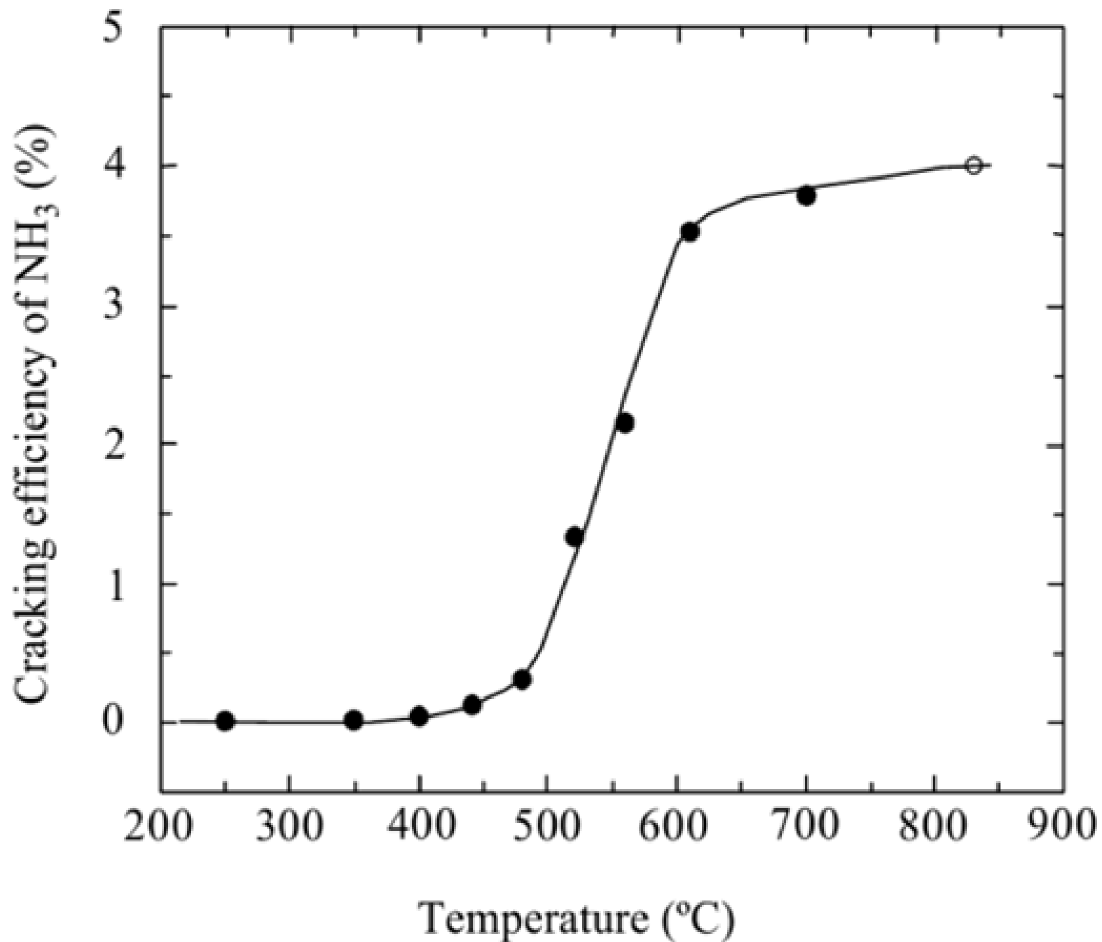

Figure.8: Thermal decomposition efficiency of ammonia. The sudden onset of cracking efficiency sets a lower limit on temperature in nitride growths [59].

MBE provides high quality quantum well, high control over binary and ternary alloy composition structure and super lattice structure due to the control provided by effusion cell, less chemical complexes and high vacuum environment. Reflection high energy diffraction (RHEED) measurement is enhanced by UHV environment thus providing to understand the kinetic of crystal growth during the process. The quality and control of growth is great advantage offered by MBE but the equipment is relatively expensive thus limiting the growth rate and commercial production. Figure.9 shows the MBE model with several effusion cells with each having individual shutter and line of sight to the substrate. The RHEED gun setup can be seen in the figure where the electron beam is directed to the substrate surface. The main valve is on the right hand side of the chamber as show in the figure.

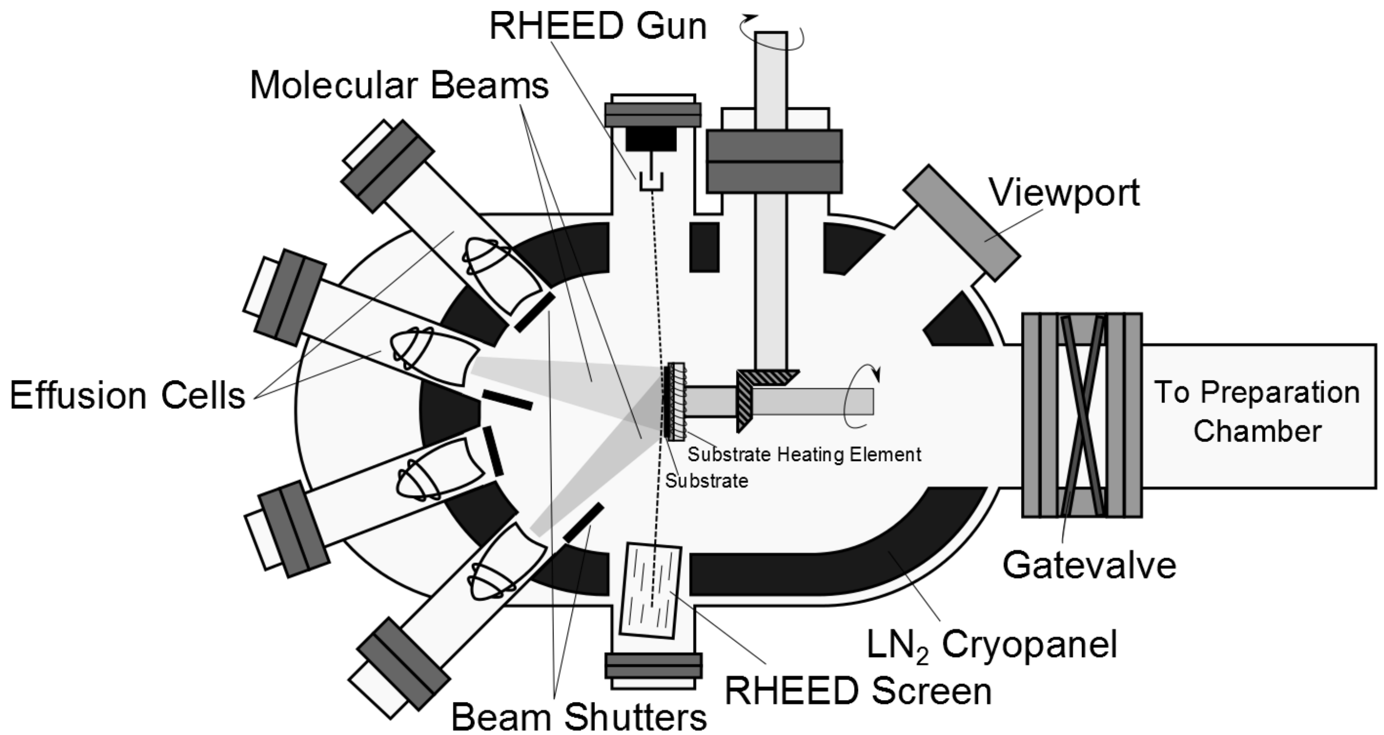

Figure.9: Typical MBE deposition chamber [60].

3.2.5 MOCVD

Metal Organic Chemical Vapour Deposition (MOCVD) is a growth deposition method similar to ALD but it depends completely on full thermal decomposition of the metal organic precursors. The precursor used for the growth process in the method are metal organic which contain metal carbon bond. Typically for III-V nitride growth process trimethylgallium (TMGa), trimethylaluminium (TMAl) and trimethylindium (TMIn) is used as precursors along with nitrogen. As we have seen previously ammonia is used as nitrogen precursor in MBE with thermally limited reaction. MOCVD operates at higher temperature compared to ALD and at moderate pressure in comparison with MBE. For

full pyrolysis of metal organic precursor in MOCVD higher temperature is used which is complete opposite to ALD where ligand exchange occurs. Indicating the deposition reaction is not just limited to surface and with in the chamber the reaction occur in gas phase. The higher temperature and pressure present in the chamber result in a boundary volume above the substrate. The precursor vapour phase decomposition occur at this boundary region. Due to this boundary level, three growth regimes exists for the deposition method. At lower temperature growth will be restricted to the rate at which the ligands can be moved from the metal atom. This rate is given by Arrhenius equation, thus kinetically the growth is limited at this temperature due to thin boundary layer and diffusion occurs quickly. As the temperature increases, boundary region extend as the heat from substrate activates precursor further distance from substrate. The diffusion of precursor consumes more time as boundary region grows thus limiting the growth step as diffusion time is comparatively long enough. This is termed as diffusion limited regime. As the temperature increase more the parasitic vapour reaction and evaporation dominates the growth deposition there by the growth rate decreases. This limitation varies between deposition pressure and precursors. MOCVD has many advantages compared with other deposition method. It can produce uniform layers even with complex geometry and no limitation with line of sight like physical deposition.

3.2.6 Plasma Assisted Growth technique

Ammonia has been used as nitrogen source irrespective of the deposition method used for the growth of III-V nitride semiconductor. To obtain reasonable levels of nitrogen incorporating in crystal lattice ammonia forces a limitation on the growth temperature as to break N-H bonds sufficient thermal energy must be provided. When this samples are grown at lower temperature the chance of nitrogen acting as donor is high due to the formation of nitrogen vacancies. This is a big issue when we need to grow p-type and intrinsic layer. To over come this issue we can provide energy to nitrogen molecule alternatively by an electric and time varying magnetic field. By this alternative method the growth can be achieved at lower temperature. Plasma is an environment filled with ionized gas. To generate nitrogen plasma, nitrogen gas is passed through high field so that the gas molecules are ionized. The velocity of electron in plasma is given by Maxwell Boltzmann distribution and to dissociate nitrogen small fraction of electron energy is enough. Providing atomic nitrogen species and molecular nitrogen in addition to small content of ionic species. The electrons generated from ionization are called hot electrons as they have high kinetic energy. In comparison with temperature of the system and relative mass of the atom, the kinetic energy of the gas atom is small. Plasma sheath is resulted due to non-equilibrium condition of the hot electrons. Electrons expand at a greater rate than ions because of the high kinetic energy and charge the surface negatively in contact with the

plasma. When the attractive force of ions impacts the hot electron flux, the plasma bulk and surface reach steady state. The ions are accelerated at different potential and plasma assisted growth is effected by kinetic energy of this ions. Figure.10 shows the outline of the effect [61]

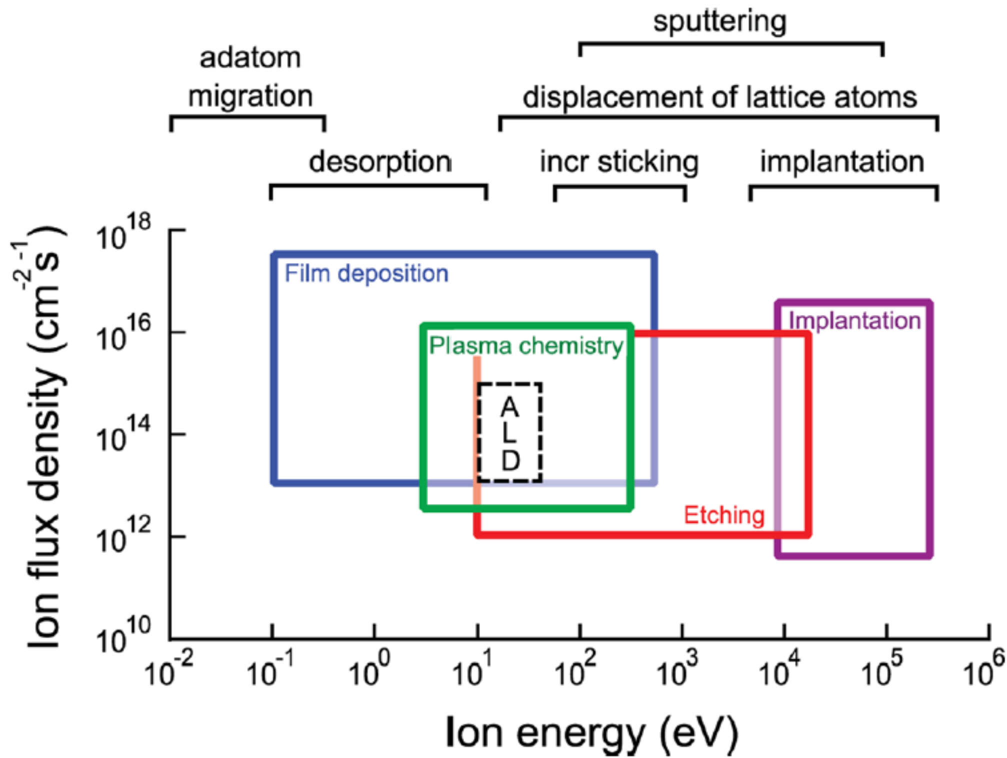

Figure.10: Possible effects of high energy ions on ALD growths. These effects are not specific to ALD and directly apply to both MBE and MOCVD techniques [73].

The effect of these ions are advantageous at low energy, helps in migration of adatom during the deposition and at higher energy, etching and implanting ions. The mass of the ionic species allows ion energies to spin at multiple regimes depending on the composition of the plasma. It

has been observed in literature that H_2+N_2 mixtures of plasma gives growth rate at higher quality compared with pure nitrogen in nitrides for this reason [62]. For nitrogen growth the reactive species can be used as a nitrogen source but the part of each species may not be intuitive. It may be noted that growth rates can be correlated to the atomic nitrogen concentration in the plasma as every nitrogen atom in the wurtzite lattice is bonded to four metal atom but with nitrogen growth this is not observed [63]. With spectrometer the concentration of nitrogen can be measured, as each species emits a wavelength which is distinct based on the energy levels in the nitrogen. By changing power for plasma generator and chamber pressure, the composition of plasma can be controlled. In designing deposition process there is additional degree of control, but with thermally activated nitrogen process that is not possible.

3.2.7 Lakehead reactor

Lakehead reactor is a modified form of Remote Plasma Metal Organic Chemical Vapor Deposition (RPMOCVD) reactor. The system is designed with three main individual component that is pumped chambers, gas cabinet, plasma source and control panels. Along with this the system consists of load locking system, residual gas analysis chamber and a main deposition chamber. Each of the chamber is attached with mechanical rotary pump to provide required pressure for turbo pumps with high vacuum (Edwards STPH301C). The system is designed with standard UHV conflat sealing with copper gaskets. Initially samples are loaded into

the load lock by using transfer arm. In vacuum system the use of load lock is common, without depressurizing the main chamber the sample can be loaded or unloaded into the main chamber. Using MKS instruments baratron sensor and the control panel the pressure in the load lock can be monitored. There is gate valve separating load lock and main chamber, this valve is controlled by main panel. During deposition this gate valve is closed to minimize pressure change in load lock and main chamber. The main chamber consists of several monitoring tools that is RHEED gun baratron pressure sensor, thermometer, pyrometer. The main chamber pressure is controlled by baratron and throttling valve. Thermocouples and main chamber heater coil are automatically controlled during growth. Oxygen contamination can be minimized then the growth is carried out under low pressure. Main chamber consists of cathode plasma source used to generate plasma, the substrate holder which is set in rotational motion to ensure uniform deposition on the growth sample. DC power is used to generate plasma in main chamber consisting of two parallel plates acting as anode and cathode. At 600W plasma power, the electron density is $9.0x10^{11}$ cm^{-3} [63]. Quartz and alumina tube are avoided to minimize oxygen contamination. The density of gas required for plasma source is limited by growth pressure. Gas cabinet consist of source precursor used for III-V nitride growth which is controlled by main control panel. Figure.11 shows the schematic diagram of lakehead reactor. Along with III-V nitride precursor gas cabinet contain Biscyclopentadienyl

magnesium (Cp_2Mg) used for p-type doping. To control the precursor flow through vapour line into the main chamber, mass flow controller is used. To ensure a lack of contamination pneumatic valve system is used with ultra high purity nitrogen tank. System do not use carrier gas for precursor instead there is controlled pressure system on the vapour line to maintain precursor flow into main chamber. The pneumatic valve system allows fast binary flow control through vapour line via main chamber or enabling bypass valve with the required bottle valve open. With the main control software we can enable the required valve for the growth deposition. Precursors are allowed into main chamber in pulses to reduce parasitic vapour phase reactions. The valve timings for the deposition is controlled by main control panel and by growth recipe. The pulses are repeated to obtain thin film layer. Separate nitrogen tank is connected to the plasma head and the valve is controlled by flow controller. The flow of nitrogen to generate plasma in the main chamber is independent of metal organic introduction. Plasma can be generated continuously or can be pulsed by controlling the biasing voltage depending the growth requirement. The growth process can be monitored by using RHEED. RHEED electron source is developed for RHEED application in vacuum system. RHEED source generate a well collimated electron beam covering wide energy range. It works at pressure higher than 10^{-5} Torr. The electron optical parameters are chosen such that a small focus spot can be obtained, even at larger working distance the beam size remains

small, beam divergence extremely small can be obtained. The alignment of electron beam is very important. Beam deflection covers large range of angles so that any mechanical adjustment of the source in the vacuum chamber is not required.

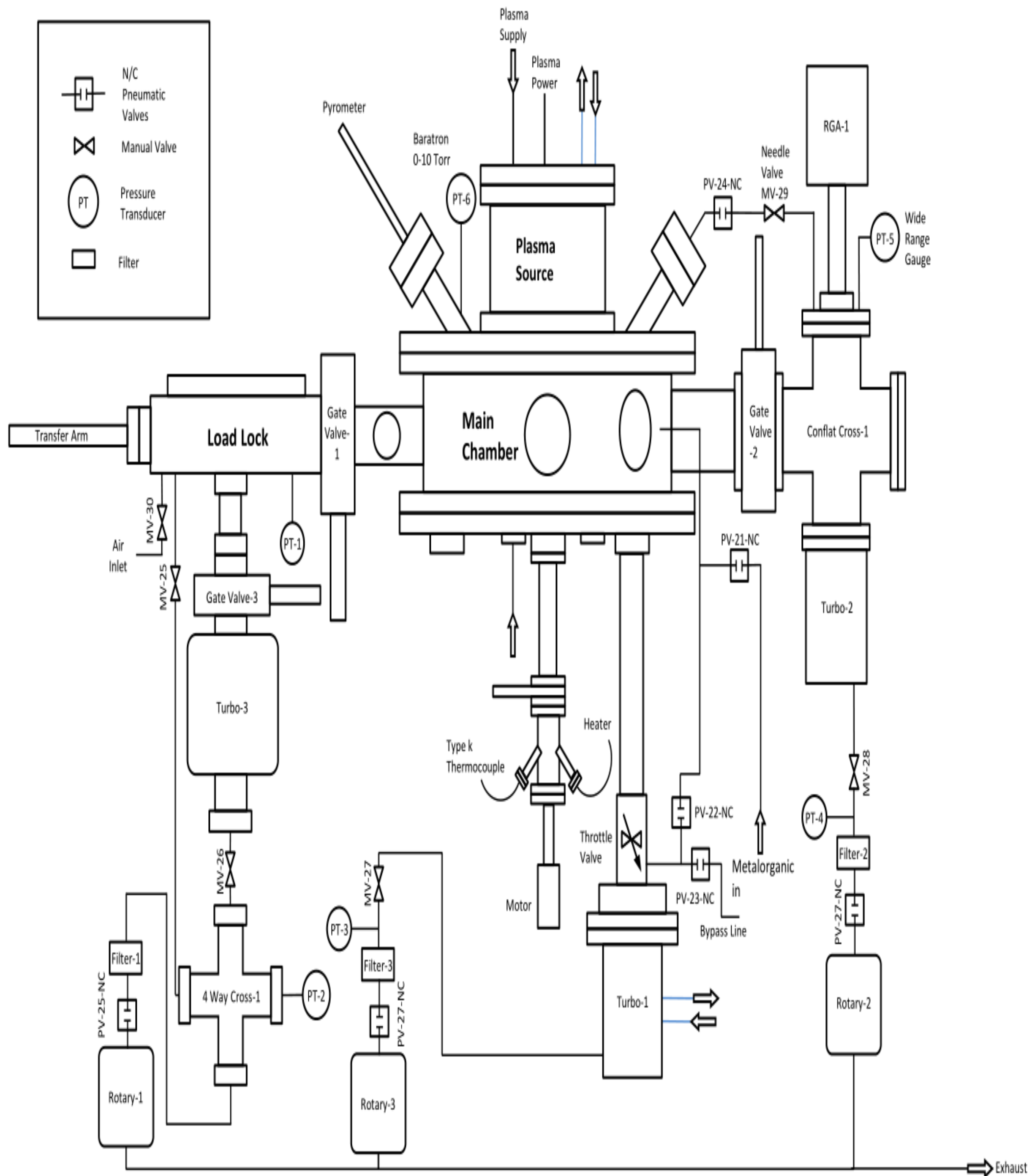

Figure.11: The gas cabinet of the Lakehead experimental reactor. This cabinet controls all gas flow to main chamber through pneumatic valves and maintains temperatures vapour flow in the lines [63]

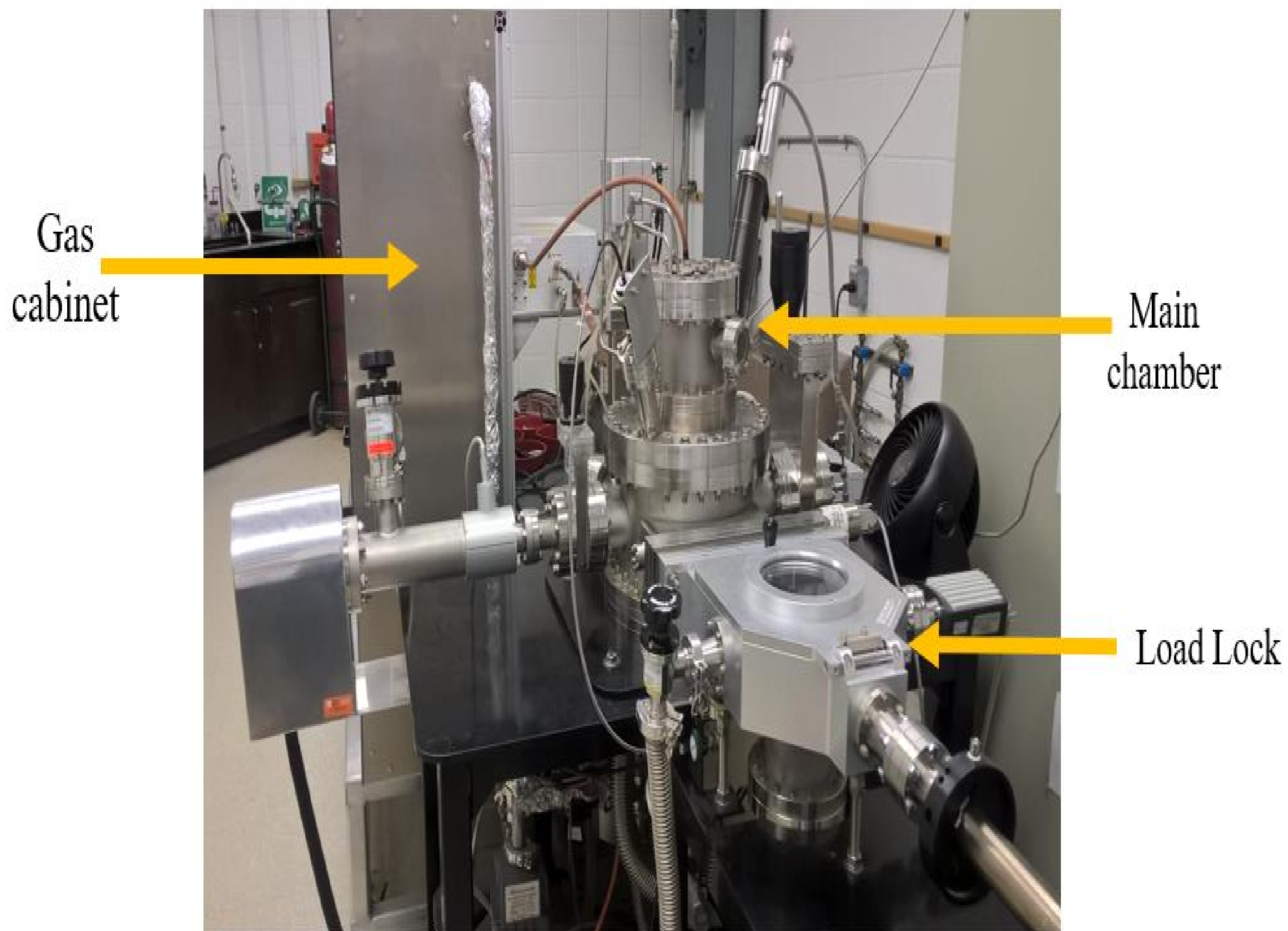

Figure.12: Lakehead University Remote Plasma-Enhanced MOCVD System

Chapter 4: Characterization techniques

4.1 X-Ray Diffraction

X-ray diffraction is a process where crystal is subjected with a x-ray radiation having a wavelength (λ) which is close to the crystal lattice as shown in the figure.13. These x-rays are obtained by bombarding a metal such as Cu with electrons in an evacuated tube [64]. Usually for the scan monochromatic x-rays are considered. These x-rays are scattered by the electron cloud surrounding each atom in the crystal. The scarred x-ray undergoes constructive interference when the path difference AB($n\lambda$) is equal to 2dsinθ (figure 13). This is the basis of Bragg's law that provides a relationship with spacing between the planes of atom at which diffraction take place (d) to the angle (θ) at which the monochromatic incident beam must focus the plane to obtain constructive interference:

$$n\lambda = 2d \sin \theta \quad (4.1a)$$

The angle 2θ is measured experimentally. The sample and detector are moved as the crystal acts like a 3D diffraction grating and a 3D array of diffraction maxima can be measured. Diffraction spot will be produced by each set of crystal planes as the shape and position of the diffraction spots being inversely related to size and spacings of the crystal planes. The crystal planes have diffraction spots with reciprocal space that form a 3D reciprocal lattice and real space. Reciprocal lattice points associated with each and every crystal plane are plotted to obtain reciprocal lattice from a

crystal. This is done by selecting an origin and drawing a vector away from the origin normal to the direction of particular set of crystal planes. The magnitude of this vector is 1/d where d is the interplanar spacing. At the end of the vector a point is plotted. The process is repeated for every set of planes until a periodic array of points has been constructed. Due to this factor, both real and reciprocal space direction remains the same but the distance might be altered. Any alteration in interplanar spacings will change the position of the diffraction spots. In figure.14 homogeneous compressive in-plane strain in GaN will increase the out-of-plane [0002] interplanar spacings due to the poisson response of the crystal in turn reducing the distance from the origin to the [0002] spot in a reciprocal space. A four index (hkil) notation is often used in a hexagonal crystal system [65]. The redundant index i equals to –(h+k) which shows the equivalency of the planes such as [$\bar{2}110$] and [$11\bar{2}0$]. Table.3 provides summary of notation conventions.

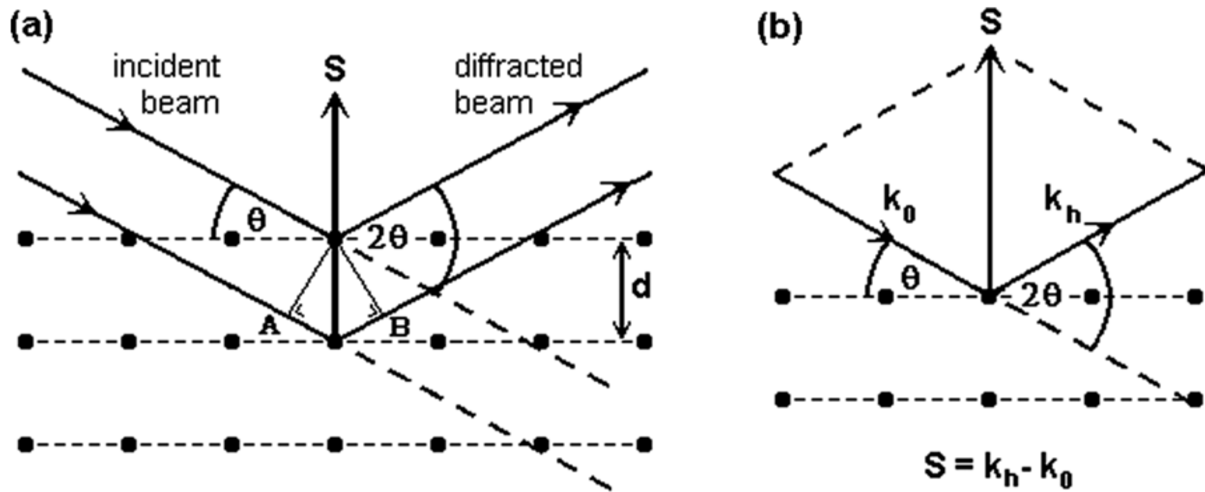

Figure.13: X-ray diffraction schematic (a) illustration of the conditions required for Bragg diffraction to occur and (b) relationship of the incident (k0), diffracted (kh) and scattering (S) vectors with respect to the crystal. Planes of atoms are indicated by dotted lines; these are not necessarily parallel to the sample surface [66]

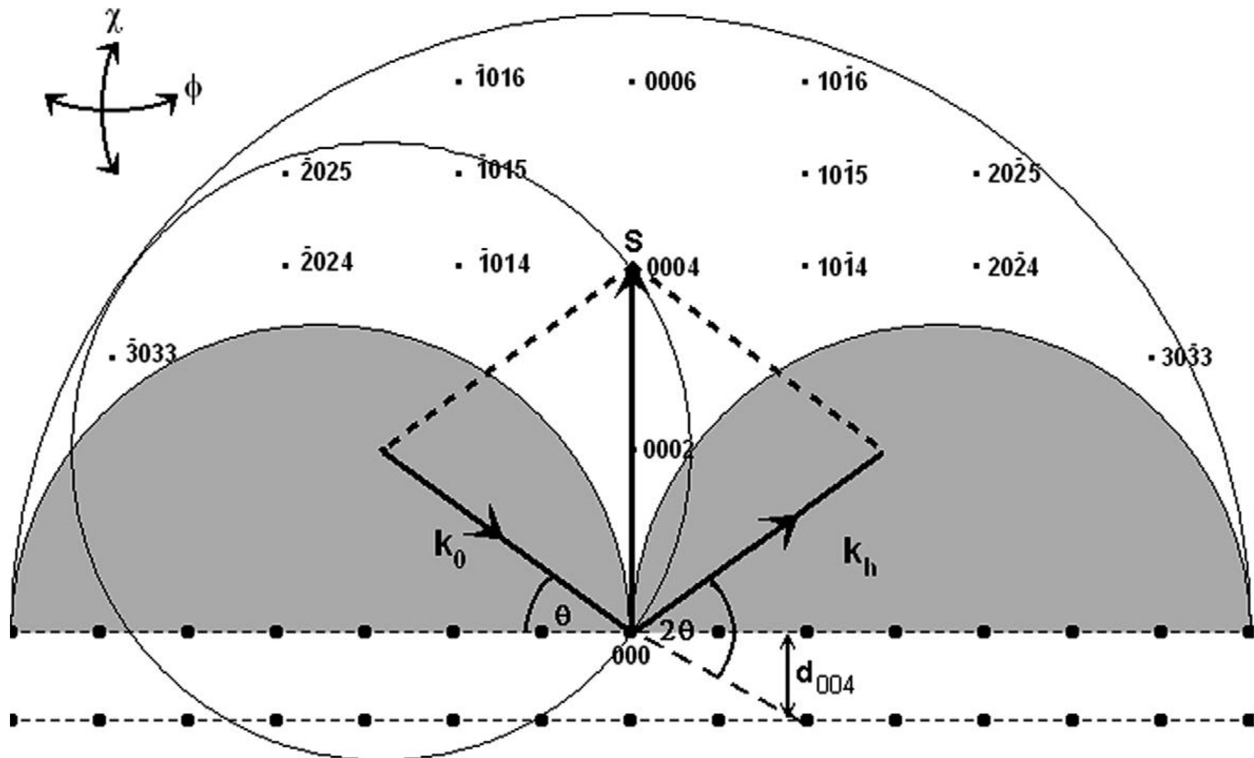

Figure.14: A section through reciprocal space for an [0001]-oriented GaN film. Regions of reciprocal space where the sample blocks a beam are shown in grey (inaccessible). The vectors k_0 and k_h have the length $1/\lambda$ (where $\lambda = 1.54$ Å); the vector S has a length of $1/d$ [0004] and is perpendicular to the [0004] plane. The Ewald sphere is shown here as a circle, cutting the [0004] reciprocal lattice spot. Some spots are absent as they have an intensity of zero [67]

Diffraction can also be shown in the context of the reciprocal lattice. If the incident (k_0) and the diffracted (k_h) beam vectors makes a particular angle with respect to the crystal, the scattering vector S equal to k_h-k_0 will end at a reciprocal lattice point as shown in figure.13(b). The scattering vector S is the probe which is used to measure reciprocal lattice whose length can be altered by altering the angle 2θ. The orientation and direction of S is scanned by changing ω, the angle at which the incident beam reaches the sample surface. The value ω will varies from that of θ (angle at which the incident beam reaches the crystal plane when the planes are not parallel to the sample surface). We can measure different areas of reciprocal space by changing the crystal orientation and by altering the length of the probe S that is changing the angles ω and 2θ, if the crystal moves with respect to the incident beam. Figure.14 shows the Ewald sphere construction used to illustrate this. Along with the sphere radius $1/\lambda$ the same vector is shown which is centered at the incident beam vector k_0. At a particular wavelength λ and the angle θ we can explore S as shown in the sphere. The length of scattering vector S increases as θ increases which can go up to maximum possible length of $2/\lambda$ which is twice the length of the incident vector k_0 at which sphere touches a spot and diffraction occurs. In figure.14 the large circle shows the outer limit which can be reached with S given maximum θ and λ.

.

Three-index notation	Four-index notation	Meaning
105	10-15	Reflection
(105)	(10-15)	Plane
{105}	{10-15}	Family of planes
[105]	[10-15]	Direction
<105>	<10-15>	Family of directions

Table 3: Summary of bracketing conventions used in x-ray diffraction

4.1.1 Measurement technique

XRD measurement is obtained using Philips PanAlytical X'Pert Pro MPD in θ-2θ mode. In this particular mode the detector and emitter are kept at the same angle normal to the sample and the angles θ is varied at a specified degree per step. The accelerating voltage of 45KV and tube current 40mA with a k-α1 peak is used for the measurement. With system software k-α2 and k-β are removed out and the highest peak is obtained by k-α1.

4.2 Scanning Electron Microscope

The scanning electron microscope is a measuring tool used to scan sample surface by utilizing a focused beam of electrons. The scanning electron microscope images has good resolution up to 1nm. It requires very small sample preparation when compared to other technique. The electron

required for the scan are generated using a filament. This generated electron is thermionic emissions under a vacuum of 10^{-7} Torr to enhance the mean free path to practical lengths. Under high voltage electrons are accelerated and the accelerated electrons are focused through series of condenser lenses. Once the beam reaches end lens, it will be deflected in the x and y direction to produce a raster over the sample area. When the electrons hit the sample, the electron loses its energy by scattering or by absorption within the interaction volume as shown in the figure.17. The size can vary from nm to µm range depending on the electron beam power, atomic number of the element and the density.

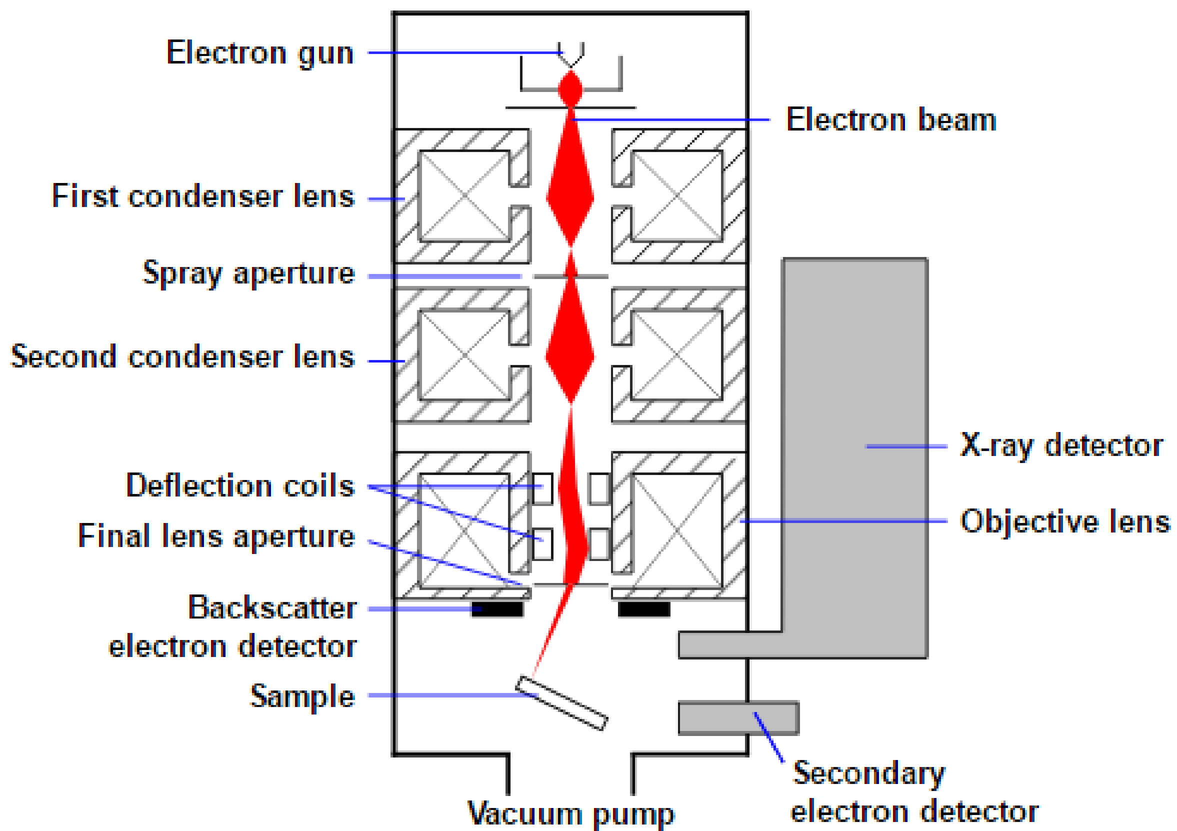

Figure 15: Schematic of a typical SEM beam and electron gun [68]

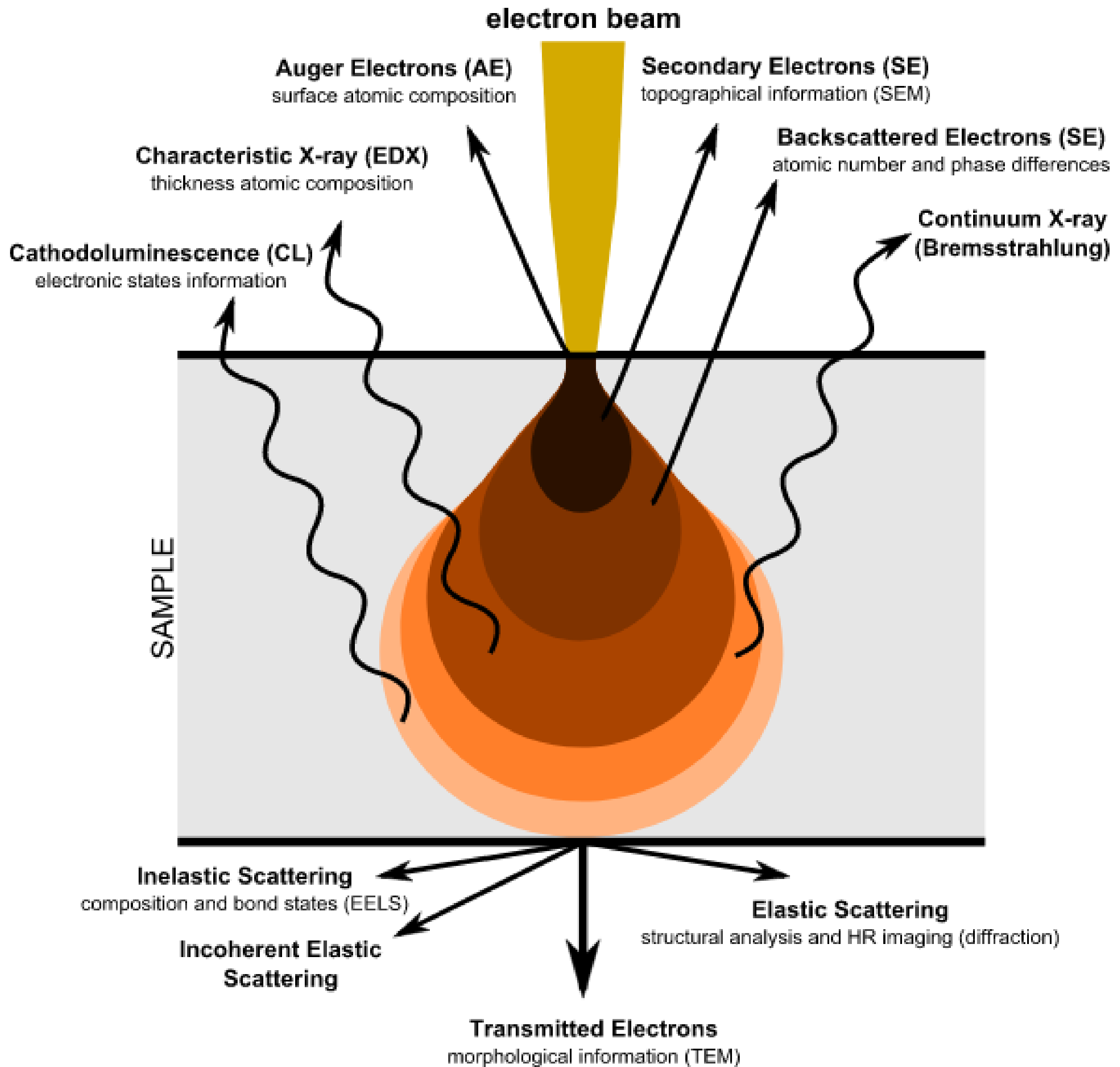

Figure 16: Interaction bloom in a sample caused by the interacting electrons. [69]

4.2.1 Measurement technique

SEM is operated under a vacuum of 10^{-5} Torr. Sample is placed inside the SEM and measurement is done using a Hitachi SU-70 located in the

university. Sample can be placed in flat position or in a holder of surface measurements or for a cross sectional views. Electrons are grounded by using conductive carbon paste or tape as an alternative carbon sputtering or copper tape can be used. Using copper or carbon increases the quality of the obtained SEM image.

4.3 Energy-dispersive X-ray Spectroscopy

EDX is used for determining elements in a sample. High energy x-ray is used for this measurement. The sample is bombarded with high energy x-ray, this excites one of the inner electrons leaving behind an electron hole. An electron from outermost higher shall slides to occupy the hole. The difference in higher and lowed energy shall is measured. EDX is done within SEM.

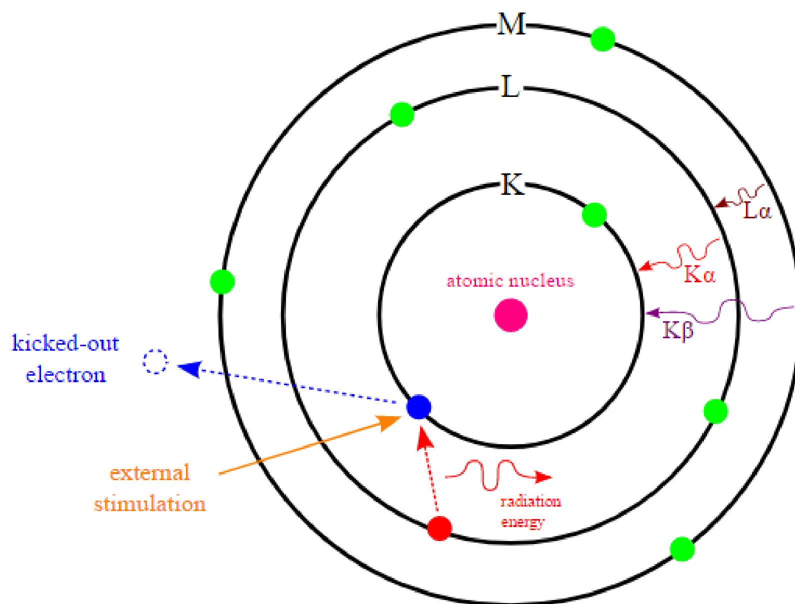

Figure 17: Schematic on how an electron is removed from the K-Shell [70]

4.4 Atomic Force Microscopy

The AFM provides atomic scale resolution of a scanned sample. It is a non-destructive surface characterization with great cost efficiency and sample preparation is very less. AFM has a small cantilever with a very fine tip which is mechanically placed over evenly spaced points in a scan area close to the sample. Using laser and photodiode array the vibrational movement of the cantilever is measured. Different data is used to estimate a false color plot of the sample depending on the operating mode. RMS surface roughness values are reported as a metric of sample smoothness. AFM are fabricated with high accurate tips on the cantilevers and control in three dimensional space of this tip position in order of one nanometer. Cantilevers are often made using silicon photolithography technology which provides precision control geometry and the thin film coatings or specific stiffness. Piezoelectric transducers are utilized for position control of the cantilever, also for macro scale movement of scan head stepper motors are used. AFM has three types of operating modes: non-contact mode, contact mode and tapping mode. In non-contact modes the cantilever is moved to its resonant frequency by bringing close to sample to experience loading due to van der waals forces. The loading is operated by laser and photodiode array which helps to shift the resonant oscillations of the probe. To adjust the distance of the probe from sample to its original position a z-axis controller is used. The sample topology is determined using controller response. The advantage of using this mode, as there is

no contact made, wear of the tip is minimised and samples which are sensitive can be measured. The disadvantage of this mode is surface contaminations. In contact mode the z-axis controller is replaced by static deflection of the probe. To maintain constant repulsive force from probe to sample z-axis controller is adjust. To define the deflection a force set point is given to the controller. To calculate the force based on the deflection the probe stiffness properties must be specified to the controller. Force should be minimized to avoid wear on the sample and probe. Tapping mode is a replacement method for non-contact mode where with a constant amplitude the probe is excited to its resonant frequency. In tapping mode, the probe is brought close to the sample to have a contact force from the surface. With this technique there is good inherent protection from tip sample adhesion also minimization of false reading due to contamination as seen in non-contact mode. Compared to wear on the tip and sample in contact mode, tapping mode is better. AFM design is shown in figure.18.

4.4.1 Measurement technique

Sample measurement are done using an AFM NanosurfEasyscan 2 atomic force microscope. ACLA model probes are used with aluminum top coating, width of 40 micrometer, a length of 225 micrometer, height of 14-16 micrometer, tip radius of <10 nanometer and a stiffness of 36-90 N/m.

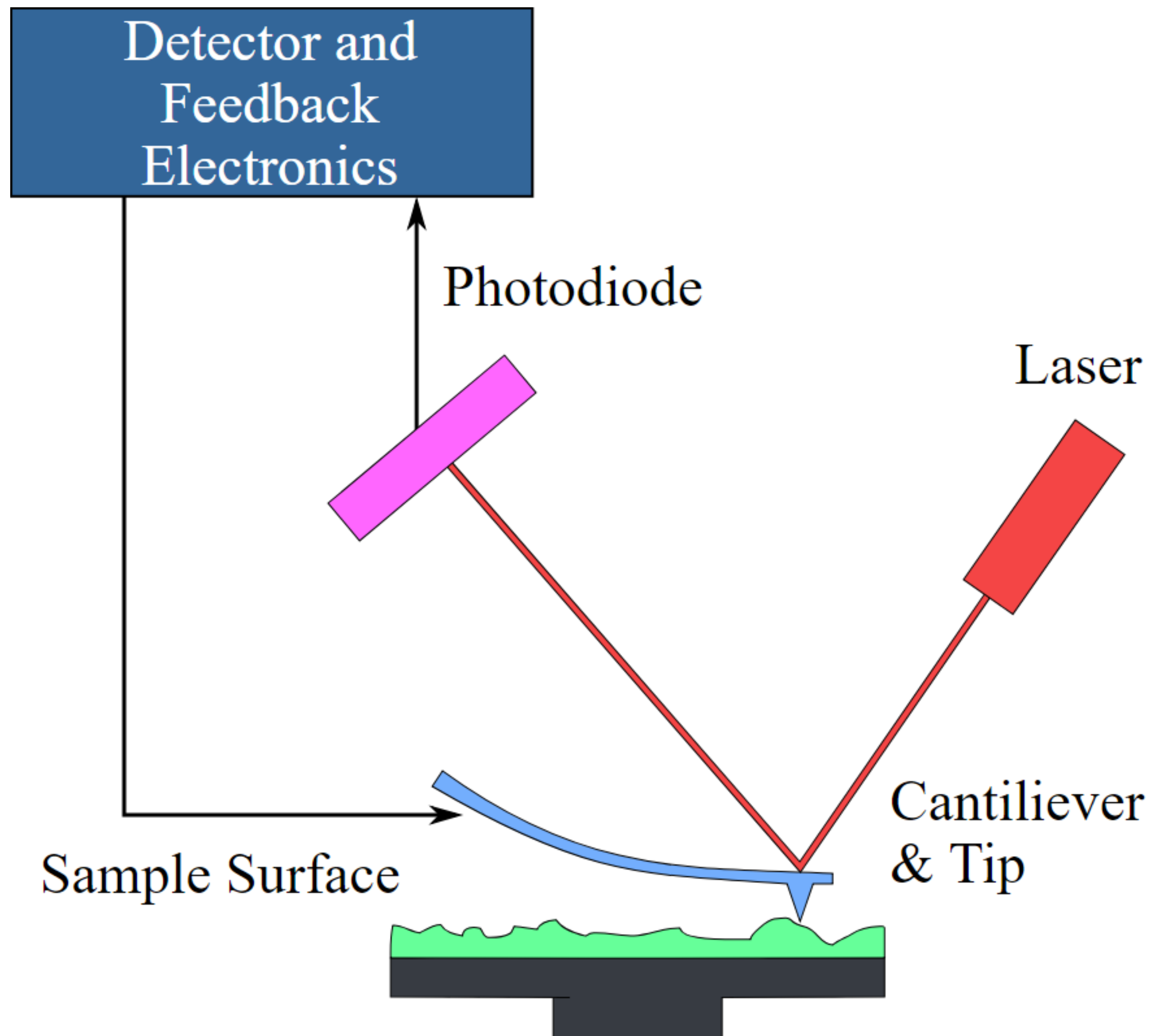

Figure.18: Schematic of typical AFM [71]

4.5 Hall Effect

Hall effect measurement is used mainly to investigate type of impurity concentration (n-type doping or p-type doping), carrier density, carrier type, resistivity, mobility of the films and electrical property of a sample. Even if the sample is not doped hall measurements is used to determine the sign and density of the majority carriers, electron mobility if the sample undoped were n-type. Figure.19 shows the hall effect measurement set up. The SI unit of Lorentz force is given by

$$F = -e (E + v \times B) \quad (4.5a)$$

According to Lorentz force when current j flows in the direction perpendicular to the magnetic field, electrical field is developed in the direction J x B. Holes and electron in the sample are forced to move in the direction perpendicular to the magnetic field. The electric field developed is called as Hall field and is given by

$$E_y = - (eB\tau E_x) / m \quad (4.5b)$$

where τ is the collision time

The Hall coefficient is defined by

$$R_H = E_y / (j \times B) = - 1 / (ne) \quad (4.5c)$$

where n is the electron concentration. This is positive for p-type doping and negative for n-type doping sample. Hall resistance is defined by

$$\rho H = BRH = Ey / jx \quad (4.5d)$$

Hall measurement which is temperature dependent can provide information about energy level of impurity within the energy gap and the impurity concentration.

4.5.1 Measurement technique

An Ecopia HMS3000DC Hall effect measurement system using Van der pauw technique is used. Electrical contacts are established on sample to be examined. Sample is mounted on sample holder, placed in between permanent dipole magnet of 1T. Current around 1nA to tens of mA is passed through the sample thus measuring the change is resistivity. First half of the measurement is done automatically later the magnet is flipped in polarity and measured again.

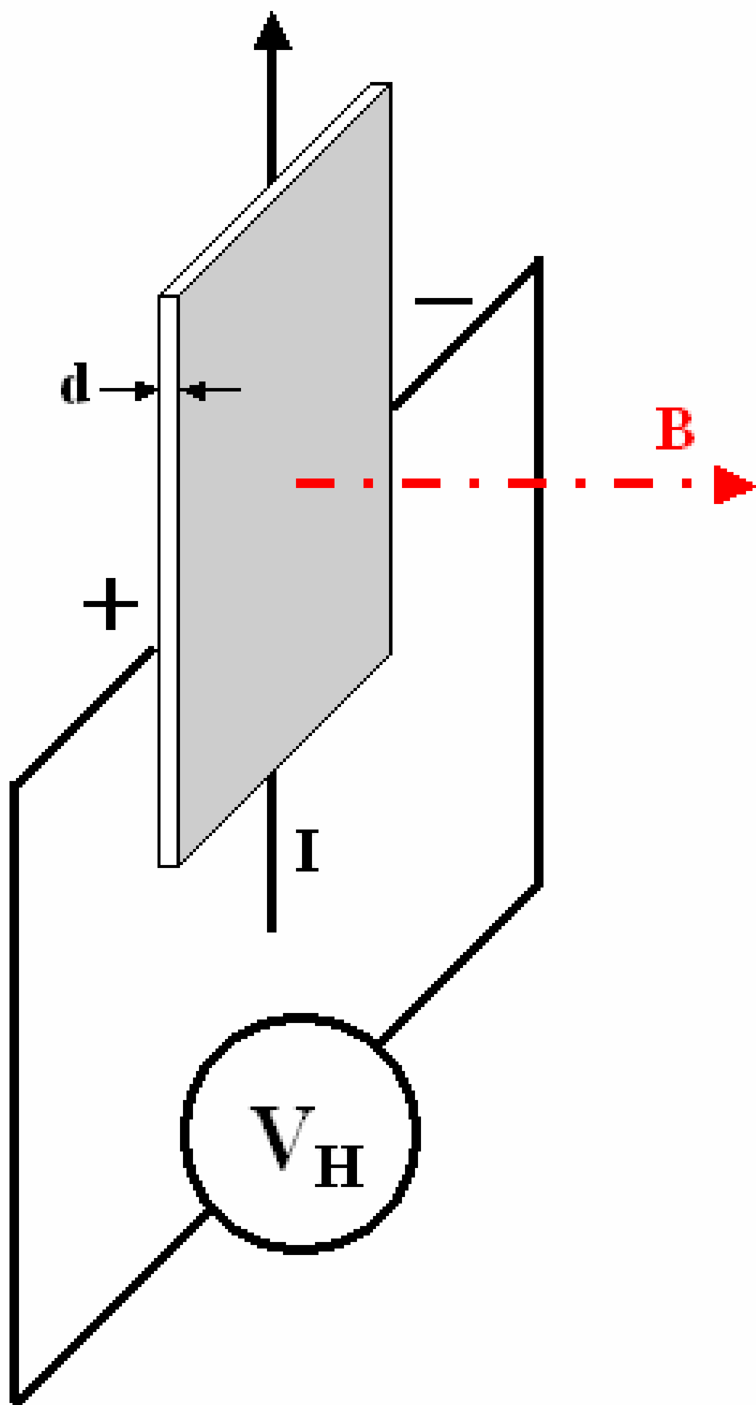

Figure.19: Schematic drawing of Hall measurement [107].

4.6 X-ray Photoelectron Spectroscopy (XPS)

XPS technique is used for surface characterization, it is also known as Electron Spectroscopy for Chemical Analysis (ESCA). XPS is surface sensitive which determines elemental and chemical composition within 2 to 10nm of the surface. Element with atomic number greater than 2 can be determined using XPS. Hydrogen and helium are not detected from XPS. Quantitative analysis of sample can be determined using XPS. By ion etching destructive depth element profiles up to several hundreds are possible with XPS. XPS is maintained at ultra high vacuum conditions. X-rays with sufficient energy are directed to the sample thus ejecting core electron from an atom. Binding energy of the electron can be determined by measuring kinetic energy of the ejected photoelectron [72]. Each element has unique binding energy which is equal to energy difference between state of electrons. Along with this auger electrons are ejected from the material.

Chapter 5: Difficulties in Mg-doped GaN

P-type doping in III-V semiconductors are achieved when group IV atoms substitute the group V atoms or group II atoms substitute the group III atoms. With GaN material system the group IV atoms such as silicon (Si), germanium (Ge) and carbon (C) does not provide p-type doping. Ge and Si acts as a donor by substituting group III atoms [74]. C is amphoteric thus it can substitute both group III and group V atom but the resultant sample will be highly resistive [75]. It has been reported that the group II elements with d-shells that is calcium and higher masses generate deep acceptor levels due to lower valance bands resonance [76]. Considering all possible options it is clear that to achieve p-type doping Mg and Be are best in match,

among them Mg has shown successful result in achieving p-type doping.

5.1 Solubility

Solubility is the most difficult aspect of doping GaN with Mg. solubility is the rate at which solute is dissolved in a solvent. When we are talking about crystalline semiconductor material solubility is the ability of a dopant to be incorporated into the lattice of the semiconductor. We can say in general that more alike a solute and solvent are, its easier for solute to dissolve in the solvent in a given material [77]. Size difference and chemical similarity between a dopant atom and host atom that the dopant atom intends to replace are the main factor that solubility depends. It has been observed that it is difficult to find impurities close to host atom thus making solubility difficult which in turn effect achieving good doping. This issue leads to

substitution of impurities on the wrong site making difficult to achieve p-type doping [78]. The low solubility limit of Mg in GaN can be expressed by comparing the limiting Mg concentration to that of N and Ga atoms in wurtzite GaN. The total concentration of N and Ga atoms in a pure wurtzite GaN can be shown as using the expression [79]

$$[\text{ GaN}] = \frac{\text{NGaN}}{\text{VGaN}} = \frac{6}{\frac{3\sqrt{3}}{2}a^2\text{c}} = \frac{12}{3\sqrt{3}(3.189X10^{-8}cm)^2(5.185X10^{-8}cm)} = 4.379\text{x}10^{22}\text{ cm}^{-3}$$

In a hexagonal close-packed (HCP) unit cell, N_{GaN} is the number of atoms in a large HCP unit cell, V_{GaN} is the large volume of HCP unit cell, a and c are lattice constant parameters for GaN [80]. It has been noted that Mg saturation limit for GaN is reached at a concentration of 10^{19} cm^{-3} [81].

Comparing the Mg concentration to the GaN atomic concentration the maximum percentage of Mg weight allowed before exceeding saturation can be found using the expression

$$\frac{\text{MMg} \;\; [\text{Mg}]}{0.5(\text{MGa} + \text{MN})\;[\text{GaN}]} = \frac{24.3\;5\text{x}10\text{E}19}{0.5(69.7 + 14)4.379\text{x}10\text{E}22} = 0.066\ \text{wt\%}$$

Where MGa, MMg and MN are the atomic masses for Ga, Mg and N respectively. With this calculation the extremely small solubility impact can be calculated. Because of this low solubility limit to achieve p-type doping, solubility is considered as limiting factor with Mg doped GaN [82].

5.2 Surface segregation and pyramidal defects

On GaN surface when Mg is introduced, Mg tends to segregate on the surface of GaN [82] by forming localized and highly concentrated areas of Mg. This segregation exceed saturation

faster when Mg is spread evenly over the surface. These highly concentrated areas can proceed to build up Mg concentration approximately to a level of 1.2 monolayers by the time surface Mg concentration is depleted by the defect formation [82]. Due to this defect the film polarity will be changed from Ga-polar films to N-polar films [83]. It has been found that Mg enhance the growth rate of GaN for particular crystallographic directions [84] and impede growth in others [85]. As a result, the formation and propagation of the defects form pyramid shaped defects with the tip pointing in the [0001] direction [86]. In hexagonal base the [0001] plane the pyramidal defect as six facets in [1213] planes [77] and are shown in figure.20. To achieve p-type doping in GaN, Mg should substitute Ga but Mg would also be bounded to surrounding N atoms by forming Mg_3N_2. Mg_3N_2 is a competing compound which is formed when high level of Mg doping is introduced in GaN [77]. Resulting in polarity inversion

of Ga-polar films to N-polar films [77]. However, if the Mg flux is lower than a Mg molar precursor ratio of 0.02 to the group III source, there is no defect found when growth is carried in MOCVD as shown in figure.21 which indicates the flux defining saturation level [82]. Above this critical flux at the beginning of the growth there is a defect free region. When the Mg concentration exceeds, at the surface Mg is depleted and form into the material through defects and this is repeated. Through out the film oscillation effect of defect concentration will be resulted as shown in figure.22 [82]. The oscillation of defect concentration is due to the buildup of Mg concentration on the surface without the presence of defects, then surface depletion of Mg through defect formation.

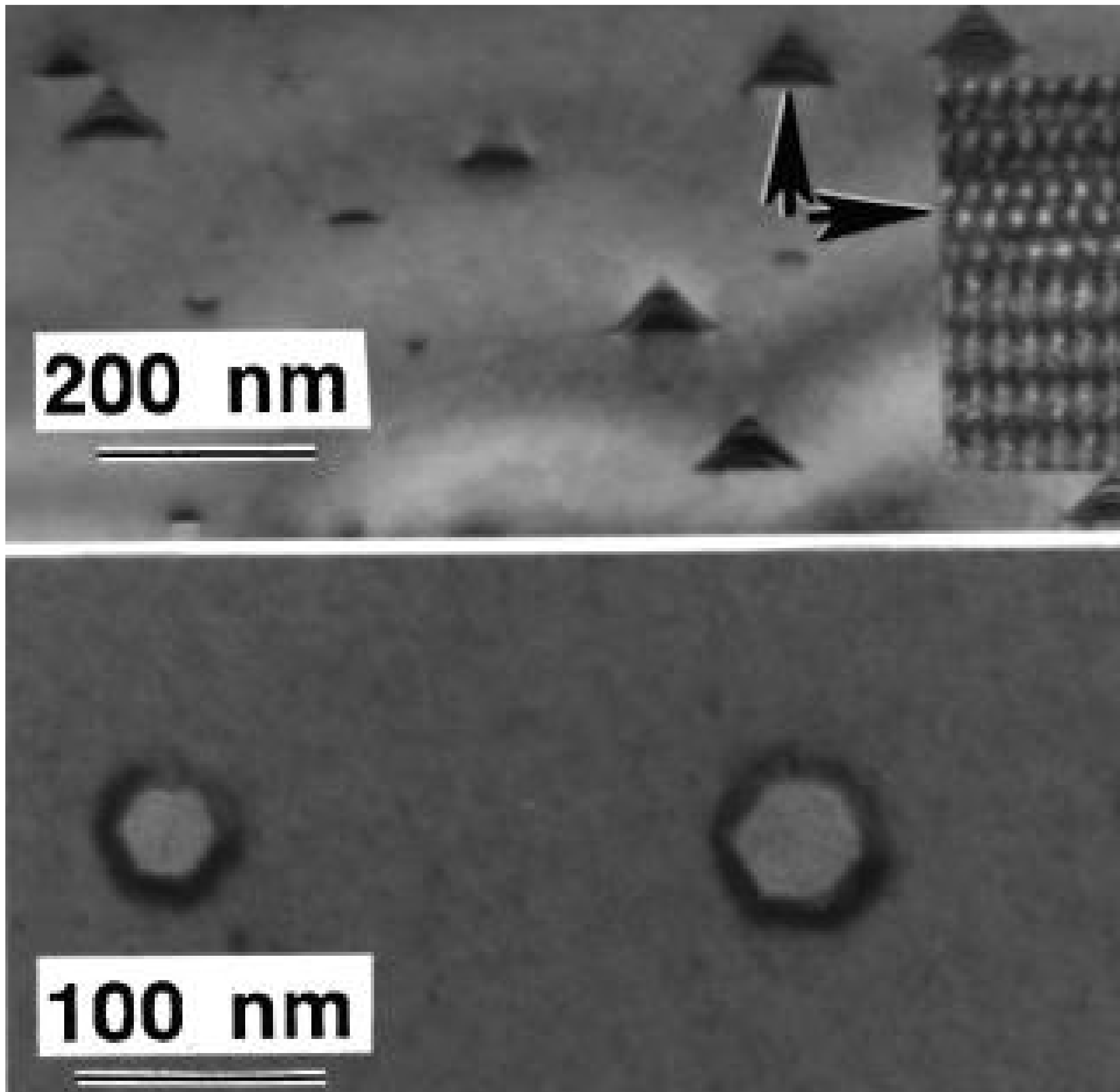

Figure 20: Cross section view of defects on top and surface view of defects on bottom [85].

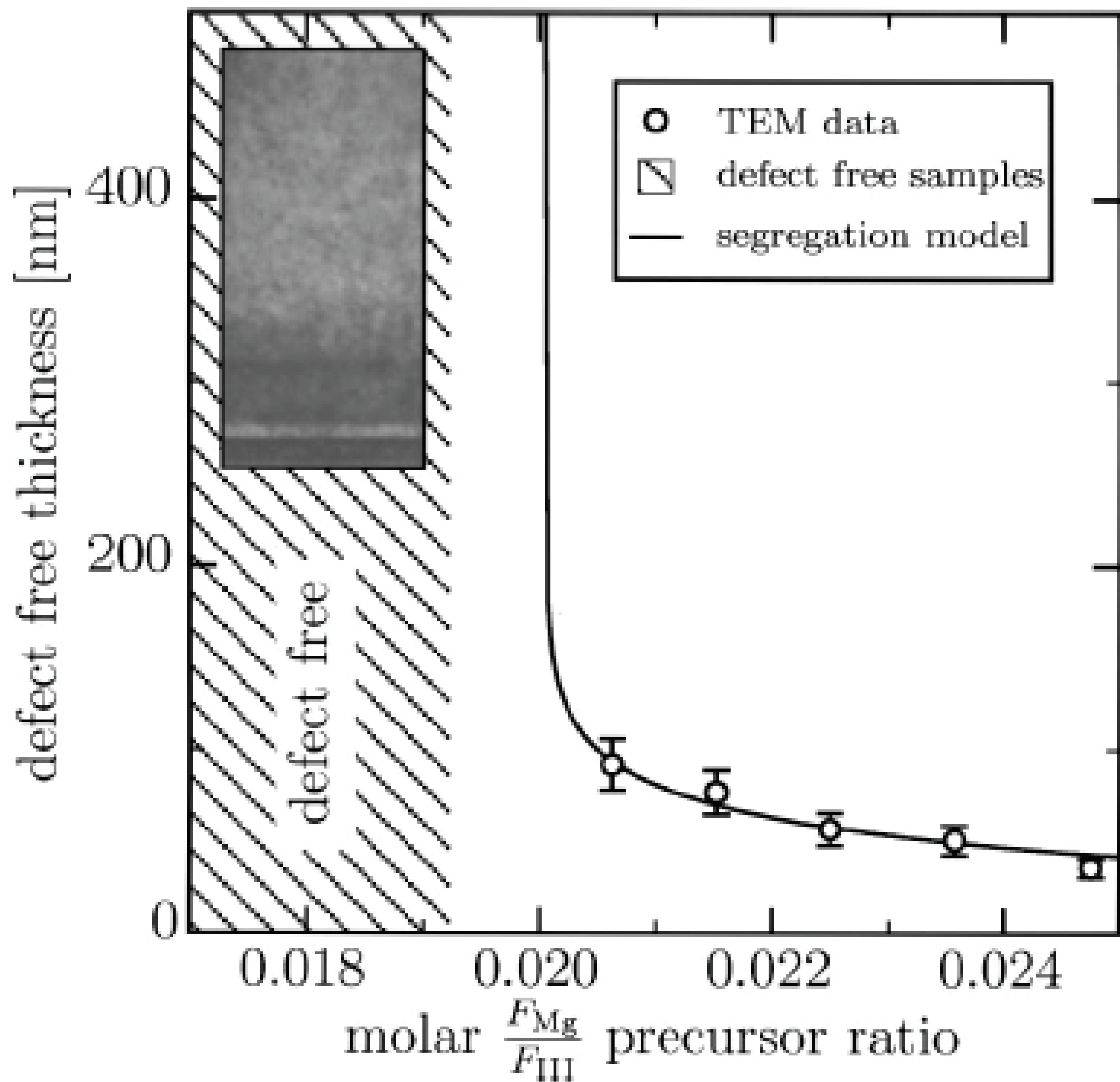

Figure.21: Response of defect-free thickness to precursor ratio, showing complete defect free growth for a molar precursor ratio less than 0.02 [85].

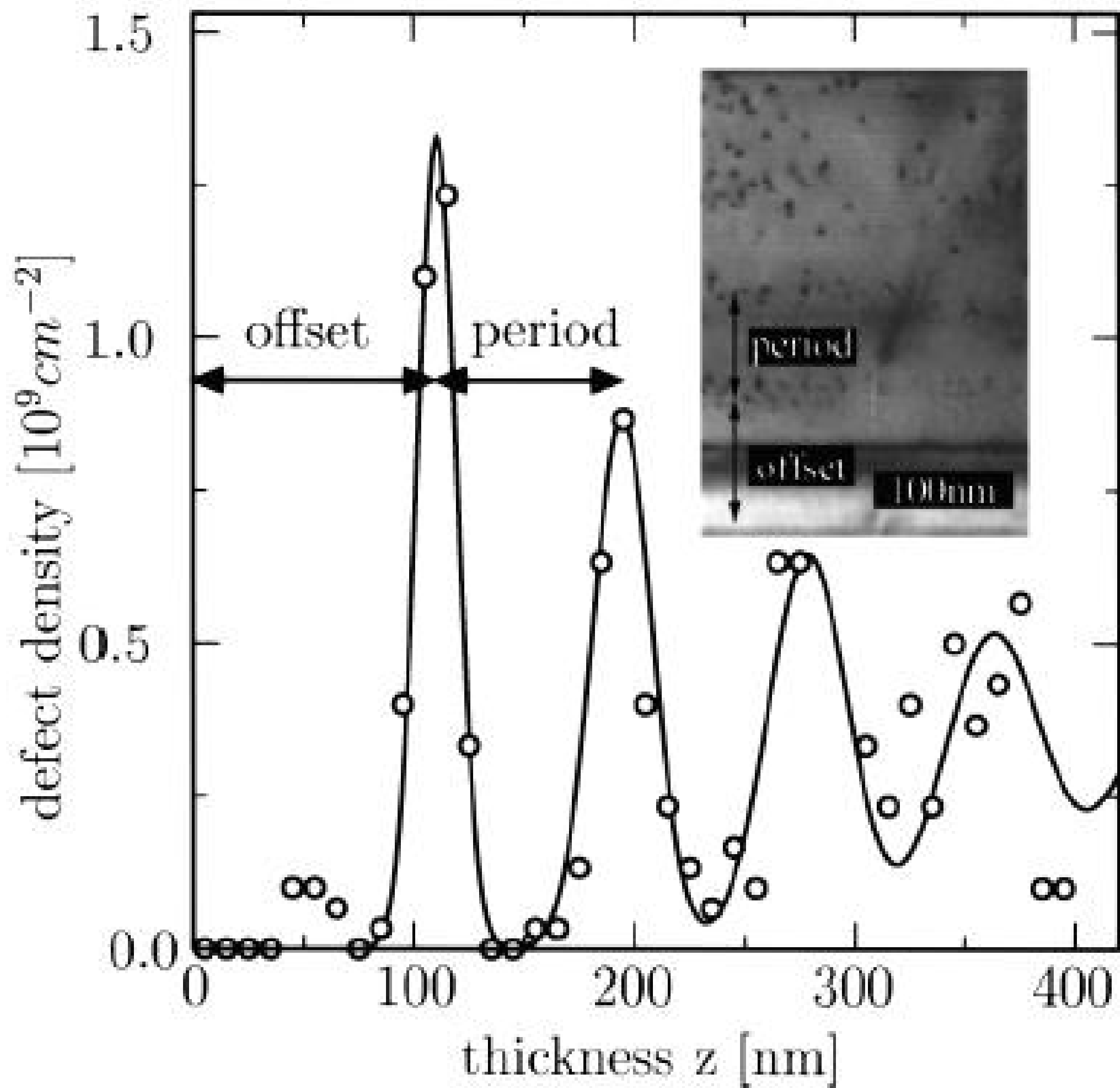

Figure.22: Relationship of defect density and thickness, showing an initial defect-free offset and following oscillation with period [85].

5.3 Memory effect

Mg source exposure exhibits a delay followed by persistence upon Mg source removal and this is known as memory effect [87]. Mg memory effect defines the tendency of Mg to accumulate on the growth chamber walls. The first Mg memory effect study was done in 1994 [87] and the similar effect was observed with Mg in GaAs [88]. It is observed, when Mg is introduced in the growth chamber a sufficient amount of Mg preferentially accumulate on walls of the growth chamber before reaching the substrate. This delay can be circumvented by keeping the substrate in waiting position out of the path of gas source then allowing Mg source. This interrupt the growth process thus allowing Mg to accumulate onto the chamber walls before starting the growth as shown in the figure.23. In reverse when Mg source is stopped allowing into the chamber the deposited Mg slowly desorbs from the growth chamber walls thus creating an unintentional Mg concentration background.

However, it has also been stated that this Mg incorporation delay is due to the result of Mg surface segregation instead of memory effect [82]. Memory effect and pyramidal defects are often an issue in CVD than for MBE. The memory effect in MBE are due to heated shutter components where Mg is re-evaporated when the Mg source shutter was closed and heated [89].

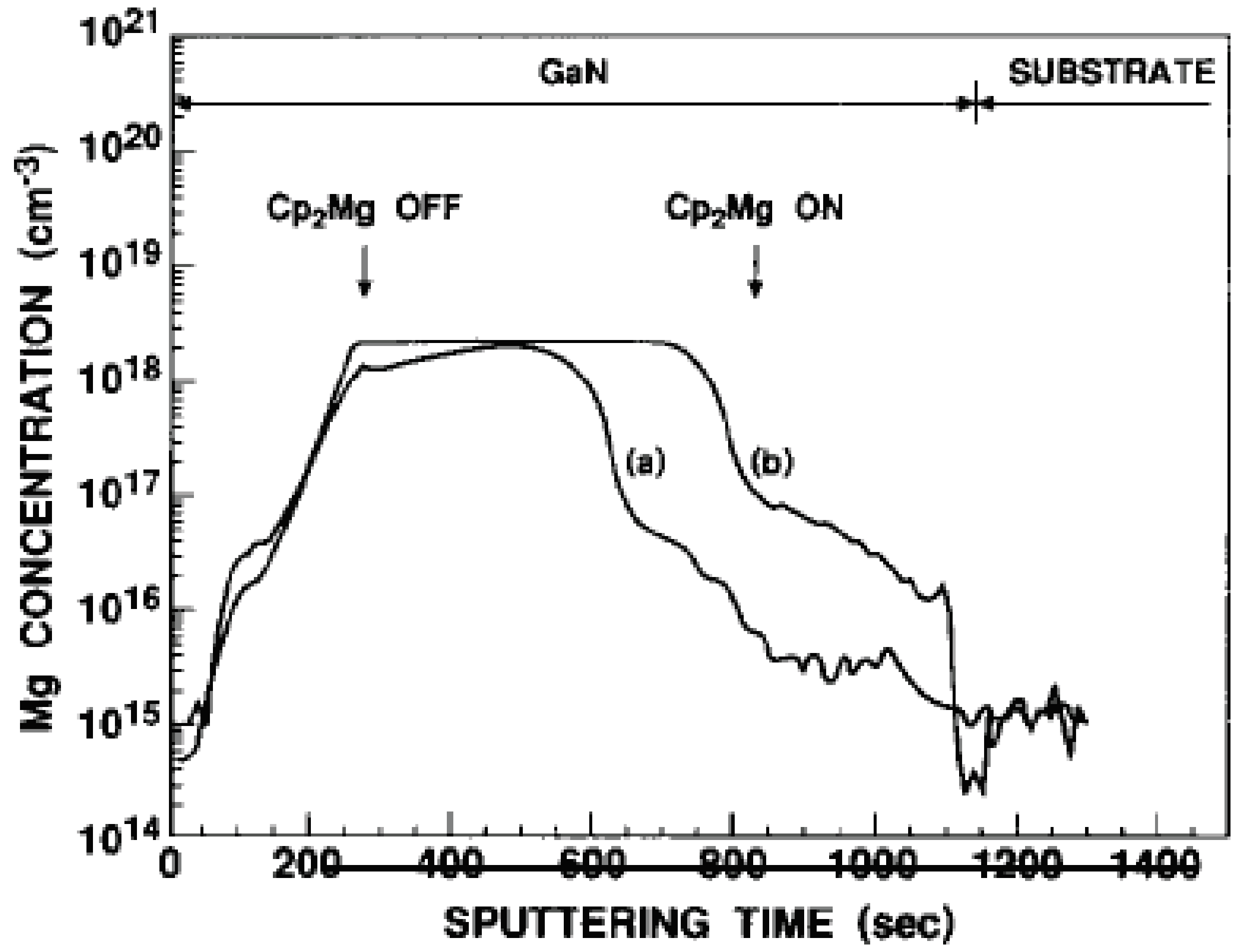

Figure.23: (a) Demonstrated memory effect of Mg-doped GaN, with (b) interruption solution showing no delay in Mg incorporation [88].

5.4 High vapor pressure

Due to ultra high vacuum environment in MBE it is difficult to control Mg dopant source. The temperature required for dopant level vapor pressure is relatively low for Mg [89]. As shown in figure.24 at low temperature the vapor pressure has large slope. The Mg flux is highly sensitive to thermal fluctuation due to this slope. Conventional effusion cells using thermal energy to control the flux of Mg is limited because of steep vapor pressure curve and due to small fluctuations in temperature leads to large fluctuations in Mg flux. The long thermal time constants with regards to temperature changes of the effusion cells, the cells can provide slow response to temperature, thus making avoidable changes in the flux of the dopant Mg a slow process.

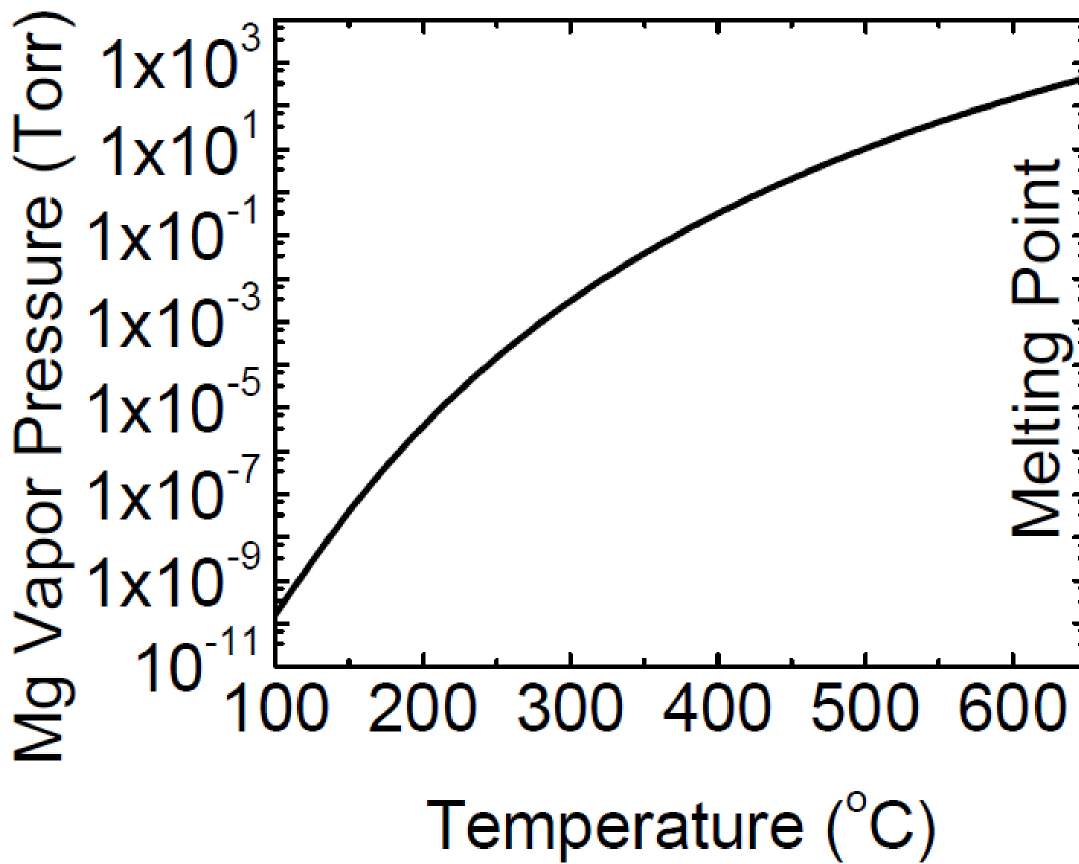

Figure.24: Vapor pressure curve for Mg [92], which shows a steep slope for low temperature, which are used for dopant-level fluxes.

5.5 Low sticking coefficient

The sticking coefficient of a particle onto a surface is the probability representation from 0 to 1 that provides the particle sticking on the surface. The required Mg flux for a specific concentration is obtained by sticking coefficient of Mg on GaN. The equation [90] gives flux from an effusion cell.

$$F = \frac{P(T)a}{\pi L^2 \sqrt{2\pi mkT}} = \frac{NA\,P(T)a}{\frac{\pi L^2 \sqrt{2\pi M}}{1000} RT}$$

$$= \frac{\left[\frac{6.022x10^{23}}{mol}\right]\left[\frac{133.3\ kg}{torr.ms^2}\right][P(T)torr][\pi\left(r^2\right)cm^2]}{\left[\frac{10000cm^2}{m^2}\right][\pi L^2 cm^2]\sqrt{\frac{2\pi(8.314)m^2.kg}{s^2.mol.kg}[\frac{kg}{1000g}][\frac{M\ g}{mol}]TK}}$$

Where NA is Avogadro's constant in mol^{-1}, a is the area of the cell in cm^2, P(T) is the equilibrium pressure in Torr at the cell

temperature T, r is the radius of the effusion cell in cm, M is the molecular mass of the evaporated species in g/mol, L is the distance from the effusion cell aperture to the substrate in cm, R is the molar gas constant in J/mol/K. without the geometric adjustments by the equation the final product can be verified for the evaporation rate of a liquid or solid surface[91]. When divided by growth rate G the dopant concentration with sticking coefficient is given by

$$\text{Ni} = \frac{r^2}{L^2} \; \frac{3.513 \; x \; 10^{22} P(T)}{G\sqrt{MT}} \; \text{cm}^{-3}$$

To find the sticking coefficient S the dopant concentration N is divided by Ni. Considering r as 0.6cm [92] and L as 13.4cm and considering remaining necessary data as an example where $G=8.33\times 10^{-9}$ cm/s, TMg = 625 K and $N \approx 8 \times 10^{17}$ at/cm^3 [88] the sticking coefficient for Mg on GaN can be found. At this Mg temperature the equilibrium vapor pressure is given approximately by 3×10^{-14} Torr [87]. Using this data, a sticking coefficient is found with the above equation.

$$S = \frac{N}{N_i} \quad \frac{N}{\frac{r^2}{L^2}\frac{3.513x10^{22}P(T)}{G\sqrt{MT}}} = \frac{8x10^7}{\frac{0.6^2}{13.4^2}\frac{3.513x10^{22}(3x10^{-4})}{8.33x10^{-9}\sqrt{(24.3)(625)}}}$$

$$= \frac{8x10^{17}}{2.06x10^{22}} = 3.88\text{x}10^{-5}$$

This result holds good for MBE growth of Mg doped GaN with solid dopant source Mg which is evaporated. As we can see the sticking coefficient is low for Mg on GaN but the sticking coefficient is high in metalorganic chemical vapor deposition [92].

5.6 High ionization energy

Once all the above defects are over come the next issue comes with freeing the hole or activating the Mg acceptor. The ionization energy or binding energy is the minimum amount of

energy required to remove the electron which is loosely held in an atom or ion. For a donor it is the energy required to remove an electron from the impurity state related with the donor to the conduction band. For an acceptor it is the energy required to remove a hole from the impurity state related with the acceptor to the valance band. For an impurity to be used as a dopant the ionization energy must be reached at the operational temperature. The impurity ionization energy has to be compared to thermal energy at room temperature KT=26meV, or less for complete ionization. The impurity will likely remain unionized if the dopant results in a much deeper impurity state than the available thermal energy even if it is perfectly soluble and perfectly incorporated in to the lattice. Using dielectric constant and effective hole mass for GaN as Kr = 9.5 [93] and m_h^*/m_0 = 0.95 to 1.1 [94] respectively the acceptor binding energy can be calculated based on that for a hydrogen atom using [43]

$E_A=13.6m_h^*/K^2_r m_0=0.143$ to 1.66 eV

Previous studies found activation energies between 112 and 190 meV [76-80] and majority of them being around 160 to 170meV [77-80] which is in good agreement with the above calculation. At room temperature this is 1% activation of Mg in GaN [78]. To completely ionize Mg acceptors a temperature over 1650°C is required. With aluminum gallium nitride (AlGaN) the activation energy of Mg acceptors is even deeper [95]. It as been reported recently that for GaN using high growth temperature the activation is as high as 10% [96] but the result is not consistent. With the high level of background electron concentration there is further limitation of low acceptor activation [97]. It is much easier to activate donors than Mg acceptors due to heavy hole mass and most of the donors will be activated at room temperature. The energy band diagram for GaN is shown in figure.25 including the donor and acceptor levels comparison with thermal energy. The standard donor concentration in GaN is 10^{16} cm^{-3} [98] but it is lower for hole concentration due to automatic compensation.

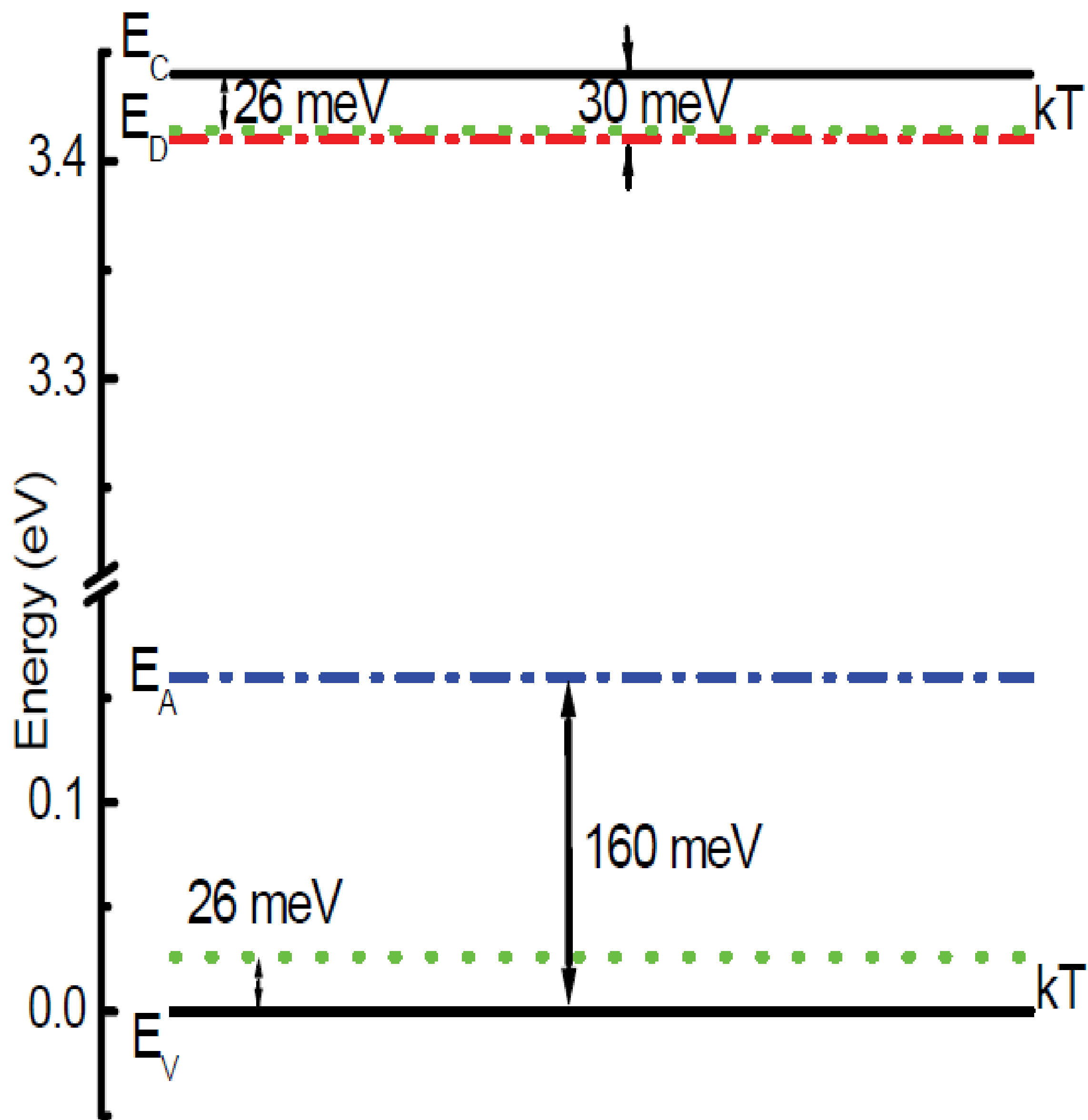

Figure 25: Energy diagram of GaN showing energy levels of donors and acceptors and the thermal energy at room temperature [97]

5.7 Unintentional dopants

From various sources, unintentional dopants are introduced into the material which limits the desirable amount of dopants incorporation. Hydrogen and oxygen are one of the sources for these unintentional dopants as it is difficult to attain ideal crystal growth condition. The equipment used for the growth also add on for unintentional doping of the material such as outgassing from particular type of heaters and fixtures [98]. It is difficult to avoid contamination in high pressure growth system such as CVD. Usually hydrogen is used as carrier gas in CVD systems, this hydrogen bond with Mg dopants in GaN thus passivating acceptor [99]. When GaN is doped more with Mg, lowering the fermi energy it is easy for hydrogen to incorporate [100]. Therefore, more hydrogen is incorporated to passivate the Mg as more Mg is incorporated without exceeding the solubility limit. Lucky the passivated Mg can be further activated by post growth treatments by liberating the H [101] which keeps fermi

level near mid-gap so that more Mg can be incorporated and activated [102]. Introduction of oxygen has been found to act as donor with an energy level of 78meV [103] thus compensating acceptor concentration. High vacuum growth systems such as MBE do not use hydrogen as carrier gas so the compensation my hydrogen and oxygen is minimal.

5.8 Compensating defects

As mentioned above doping a sample generates more free carriers and changes the fermi energy thus creating oppositely charged native defects easily. As these defects are oppositely charged the formation of compensating defects involves transfer of charges from dopants to defect or vice-versa. How Mg doped GaN suffers from this limitation is shown in figure.25 [104]. For p-type doping with low fermi energy (Ef), the formation energy for Mg to occupy Ga site as an acceptor

becomes larger than defects such as accompanying N vacancy-double donor, Mg interstitial, even a Mg N-substitutional-single donor. Thus causing limitation of hole concentration by compensating the acceptor doping. Hole concentration reduces with the increase of Mg flux [105]. Connecting back to solubility limit the Mg_3N_2 competing phase should not give either way to the doping level though formation of the compound does reduce the amount of useful Mg that can be substituted into the Ga site and lowering the hole carrier concentration. As solubility limit coincide with formation of compensation defects and the Mg_3N_2 compound [106] suggesting Mg_3N_2 acts as compensating donors.

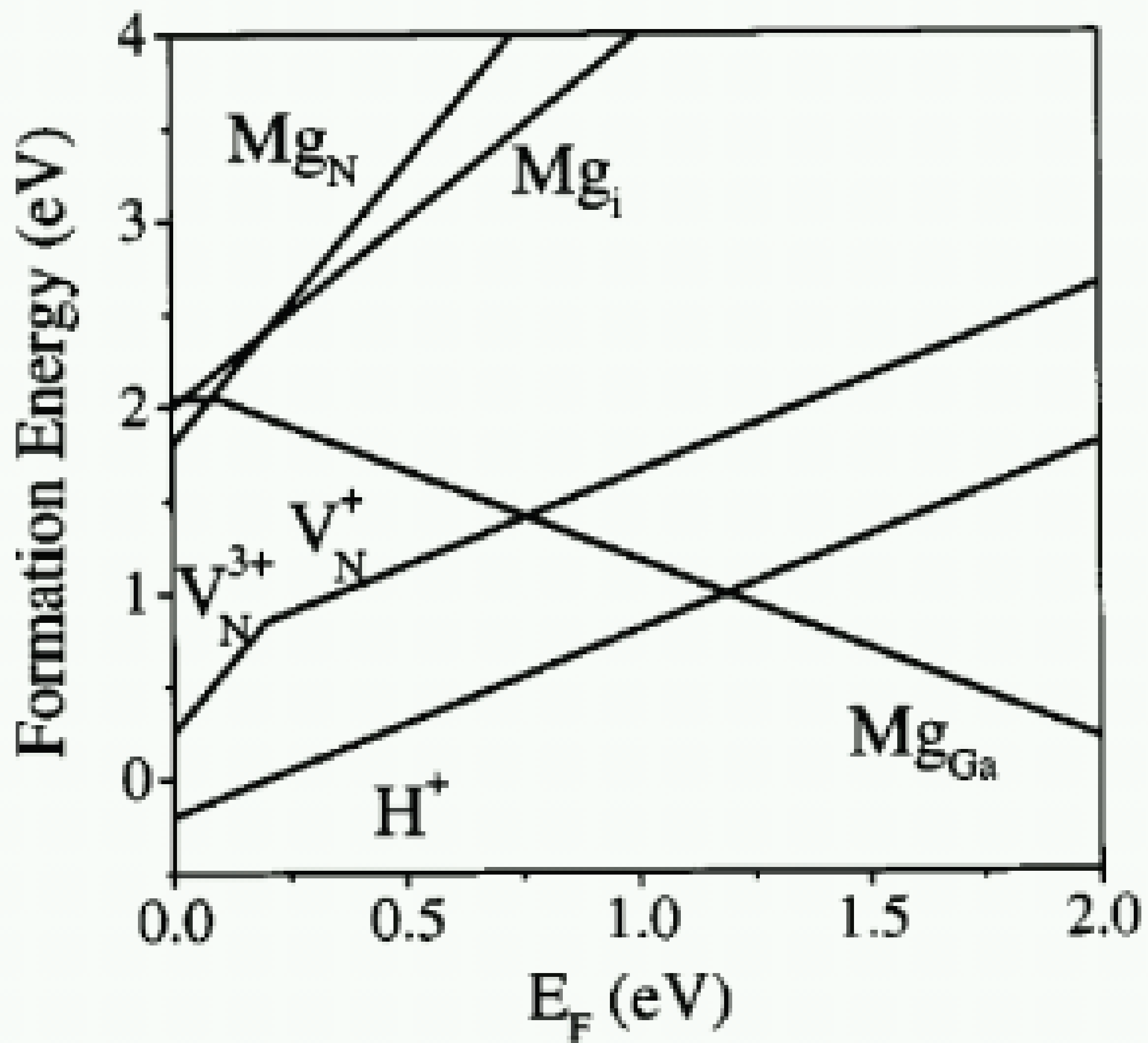

Figure 25: Formation energy as a function of Fermi level for Mg in different configurations (Ga-substitutional, N-substitutional and interstitial configuration). Vacancies and interstitial H are also included [107].

Chapter 6: Growth and Result

Growth of III-V Nitride follow same procedure

RP-MOCVD installed in Lakehead University is used to grow III-V nitride semiconductor. Main chamber is at vacuum pressure, heated initially. The heating rate is fixed, where there is 10°C rise in chamber temperature every 30s step. To minimise filament damage, the residual gas analyzer valve is closed. Manual valves for the RHEED gun and its screen used to show the RHEED result is opened during the growth to analysis the growth process. Nitrogen plasma required for III-V nitride growth is generated in main chamber by supplying power in the range 500W to 900W. Pressure in the chamber can not be changed instantaneously so the nitridation and growth pressure are varied separately. Depending on growth requirements, precursors are allowed into main chamber through vapor line. With constant flow of nitrogen into main chamber, the main chamber pressure is maintained constant. During the growth process nitrogen plasma is generated and required precursor are allowed into the growth chamber depending on the required film thickness. Until a thin film is accumulated the procedure is continued. Growth chamber is let to cool down once the growth is complete. Residual gas is removed from the main chamber through bypass line.

6.1 Growth Preparation

Before epitaxial growth of films, substrates are cleaned by ultrasonic bath with acetone and methanol for 10 minutes to remove surface contaminants. Once samples are cleaned they are transferred into the load lock by transfer arm, depressurized the load lock before opening main chamber and then placed under vacuum in main chamber. To avoid cross contamination with Sample holder it has to be cleaned before usage. Cleaning of sample holder is done with an aggressive rubbing with 120 grit sand paper, rinsing with deionized water and then methanol. Loading of the samples is done using a magnetically coupled loading arm and a viewport on the side of the reactor. Sapphire (1cm x 1cm) is used as a substrate for p-type doped GaN growth. Sapphire substrate is initially heated in main chamber to 700°C, when substrate temperature hit the required target, precursors are allowed into the main chamber. TMGa and Cp_2Mg is used as precursor for Gallium and Magnesium. Pulses of precursor and nitrogen plasma are allowed to epitaxially grow thin film of III-V nitride on sapphire substrate. Growth sample is set to cool down. Using transfer arm sample is removed from main chamber and kept in a plastic container.

6.2 Results for p-doped GaN

Experiments for deposition of p-type doped GaN are summarized in Table 4. The presence of GaN was detected by XRD, SEM, EDX and XPS analysis.

Sample	Temperature(°C)	RPM	Power(W)	TMG (Second)	Cp_2Mg (Second)	Cycle	Chamber Pressure(mTorr)
1	700	60	900	4	0	500	310
2	700	60	900	4	0	500	315
3	700	60	700	4	0	500	245
4	700	60	800	4	0	500	300
5	700	60	760	4	0	500	350
6	700	60	850	4	0	500	400
7	700	60	710	4	4	500	250
8	700	60	720	4	2	500	350
9	700	60	730	4	3	500	300
10	700	60	825	4	4	500	325

Table 4: Growth sample for p-type doped GaN

10 growth recipes of GaN and p-type GaN growths are performed on sapphire. First GaN growth is tried, later p-type doping of GaN is performed. The flow of Cp_2Mg into the main chamber is varied from 50sccm to 200sccm to determine Mg self compensation. With the increase

of Mg concentration did not show any decrease in electron concentration when measured through hall effect measurements thus making the film more resistive. The reason for this outcome was not certain. To mitigate the resistivity of film, 100sccm of Cp_2Mg was in good correlation.

Table 4 provides different growth sample performed using RP-MOCVD. Even though highest atomic nitrogen is measured at 245mTorr chamber pressure, the obtained sample 3 GaN growth result was not more crystalline. Good crystalline GaN growth were obtained at chamber pressure between 300-400mTorr. XRD result of sample 1,2,4,5,6 is shown in figure 26. The reason for good crystalline GaN grown films are due to higher average plasma powers. As the pressure in the main chamber increases, collision of molecules or ions in the main chamber is reduced as a result the deposition of epitaxial layers on the sapphire substrate becomes much easier.

GaN epitaxial results for sample 4, 5 analysed using SEM is shown in figure 27,28 and figure 31, 32. EDX result of sample 4,5 is shown in figure 29,30 and 33, 34. The oxygen and aluminum peak in the EXD result is due to sapphire substrate, carbon peak is due to carbon layer used to obtain SEM and EDX on the sample. Also, contamination could be the reason for these peaks. Thickness of epitaxial film is not even due to non-uniform deposition of GaN film on sapphire substrate.

Detection of Mg in a GaN sample using XRD or SEM is difficult. XPS is used to show the presence of Mg in GaN sample. XPS result of sample 8 is shown in figure 35. XPS peak 1303eV corresponds to Mg, 1116eV corresponds to Ga and 396.6eV to Nitrogen. To run Hall effect on Mg doped GaN sample, the sample must be highly conductive. Unfortunately, the Mg doped GaN grown using RP-MOCVD was not highly conductive and most of the case it was n-type due to Solubility, Memory effect, Surface segregation and pyramidal defects, unintentional dopants, compensating defects lacking to obtain p-type doping.

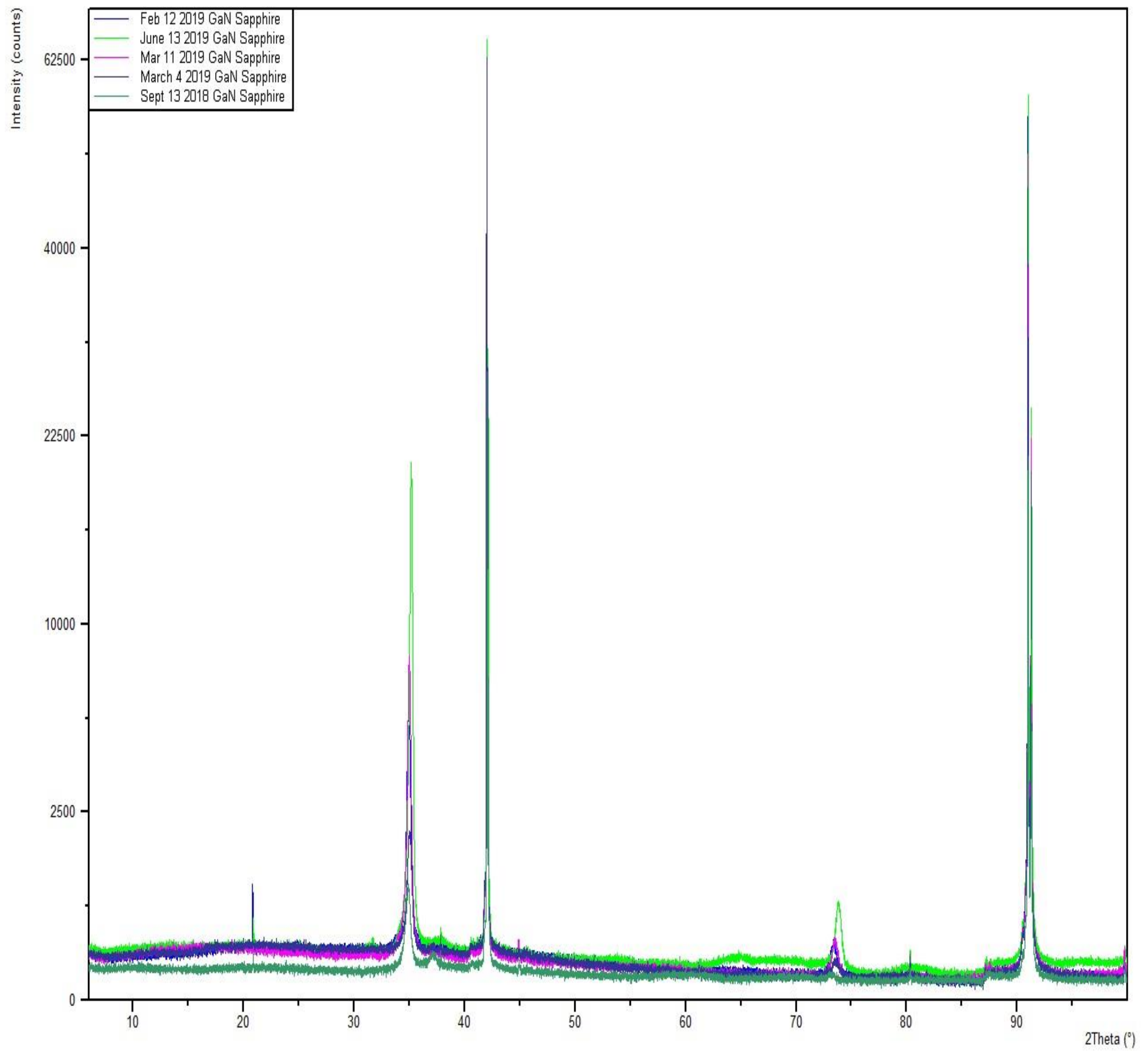

Figure 26: Combined XRD results of samples

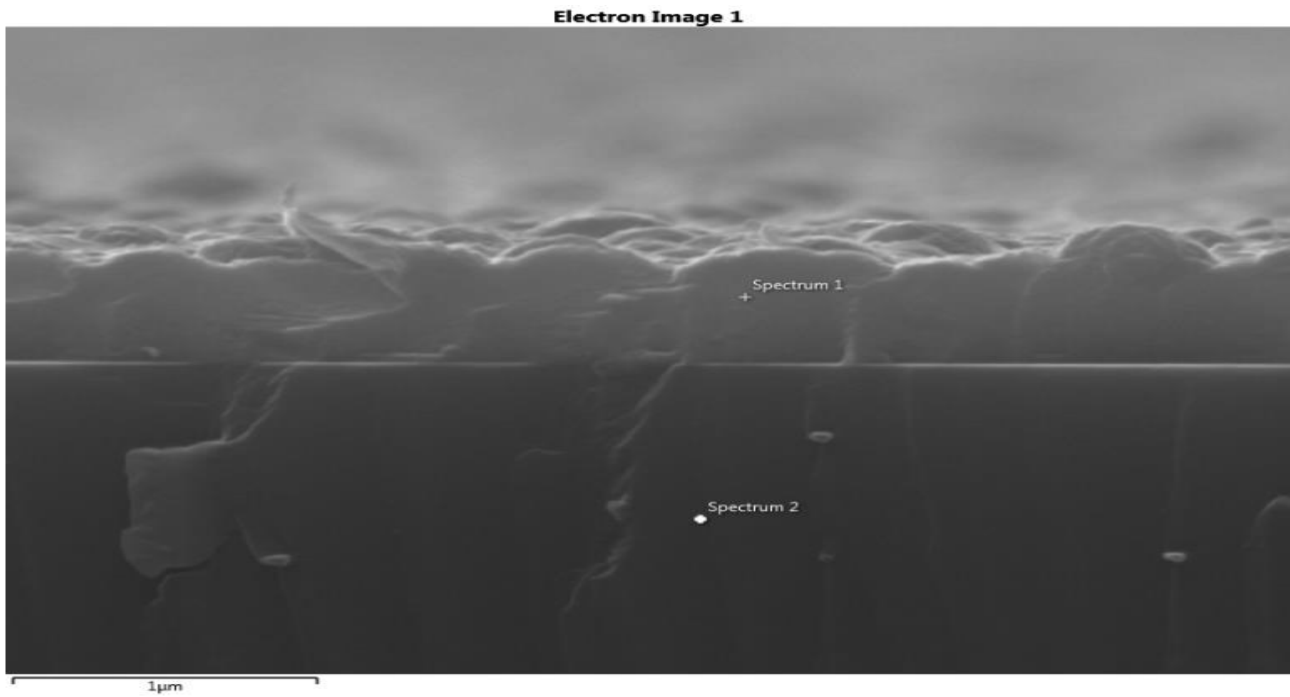

Figure 27: Cross sectional view of SEM result of sample 4

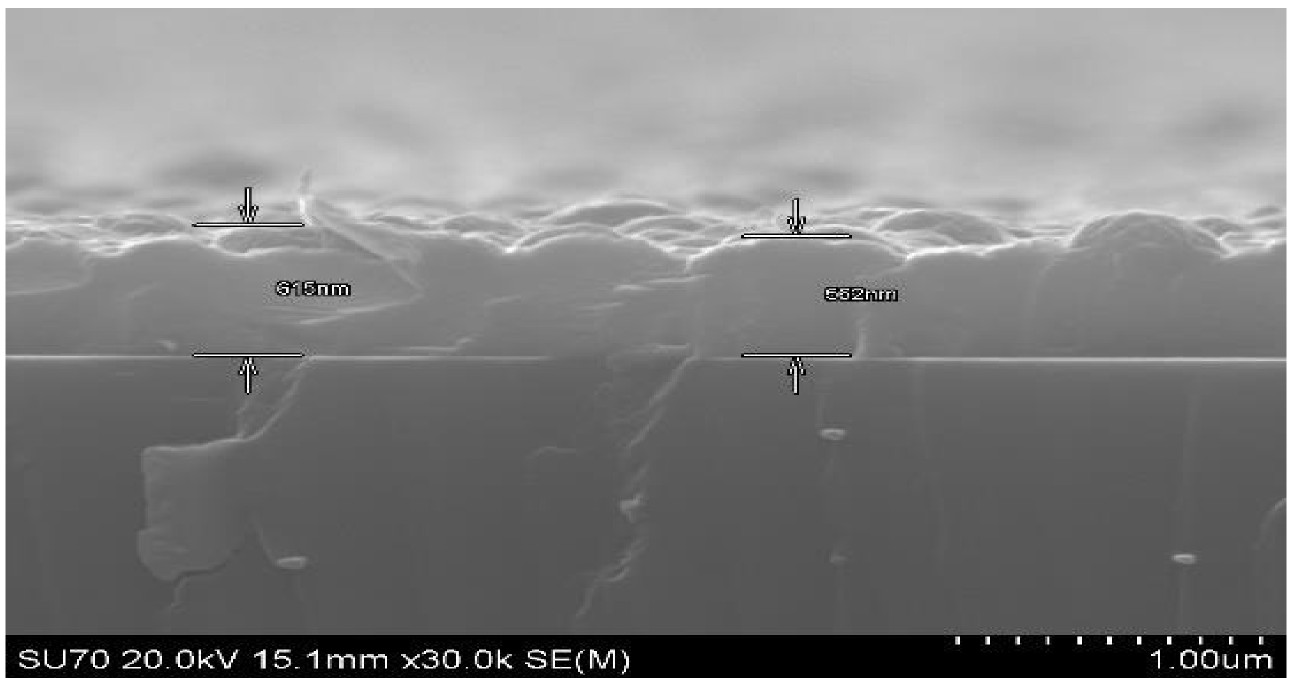

Figure 28: Cross sectional view of SEM result of sample 4 with film thickness measurement

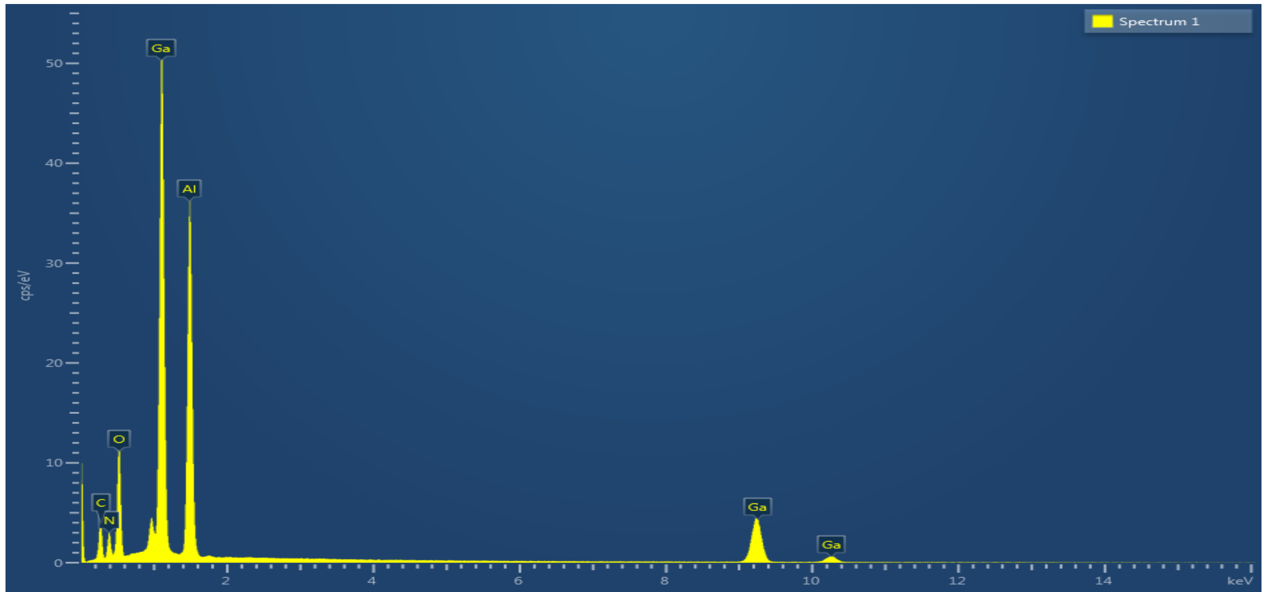

Figure 29: EDX result of sample 4 spectrum 1

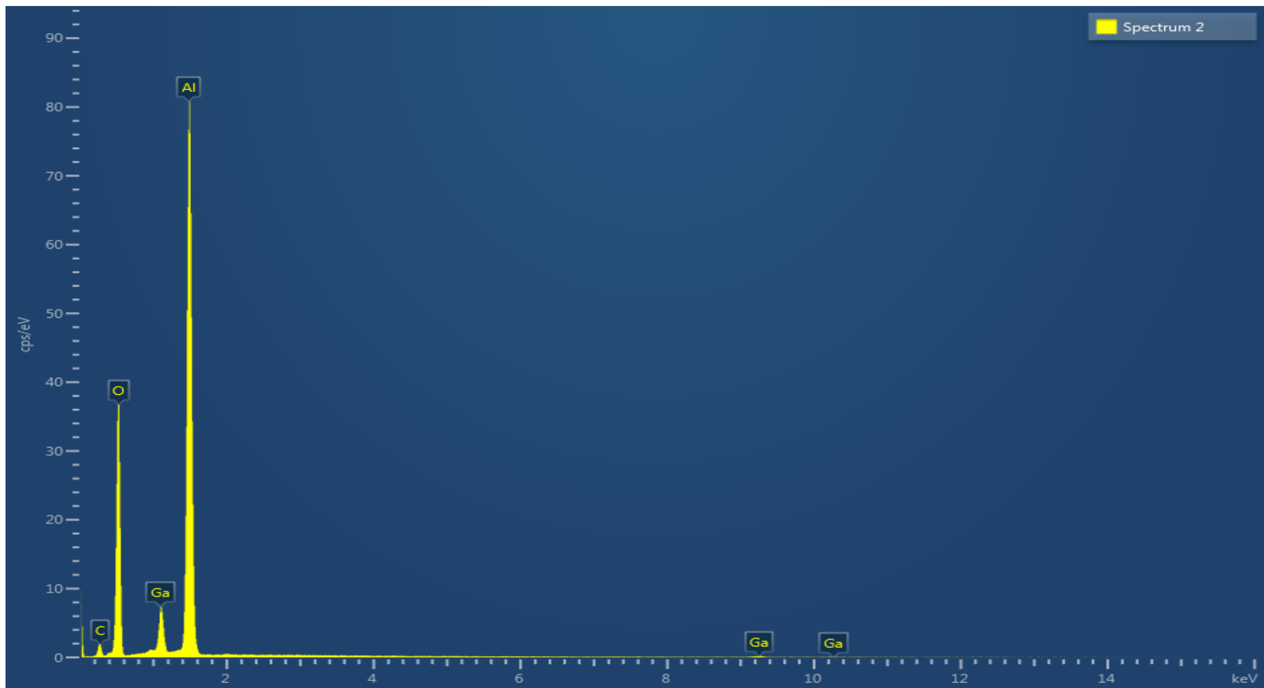

Figure 30: EDX result of sample 4 spectrum 2

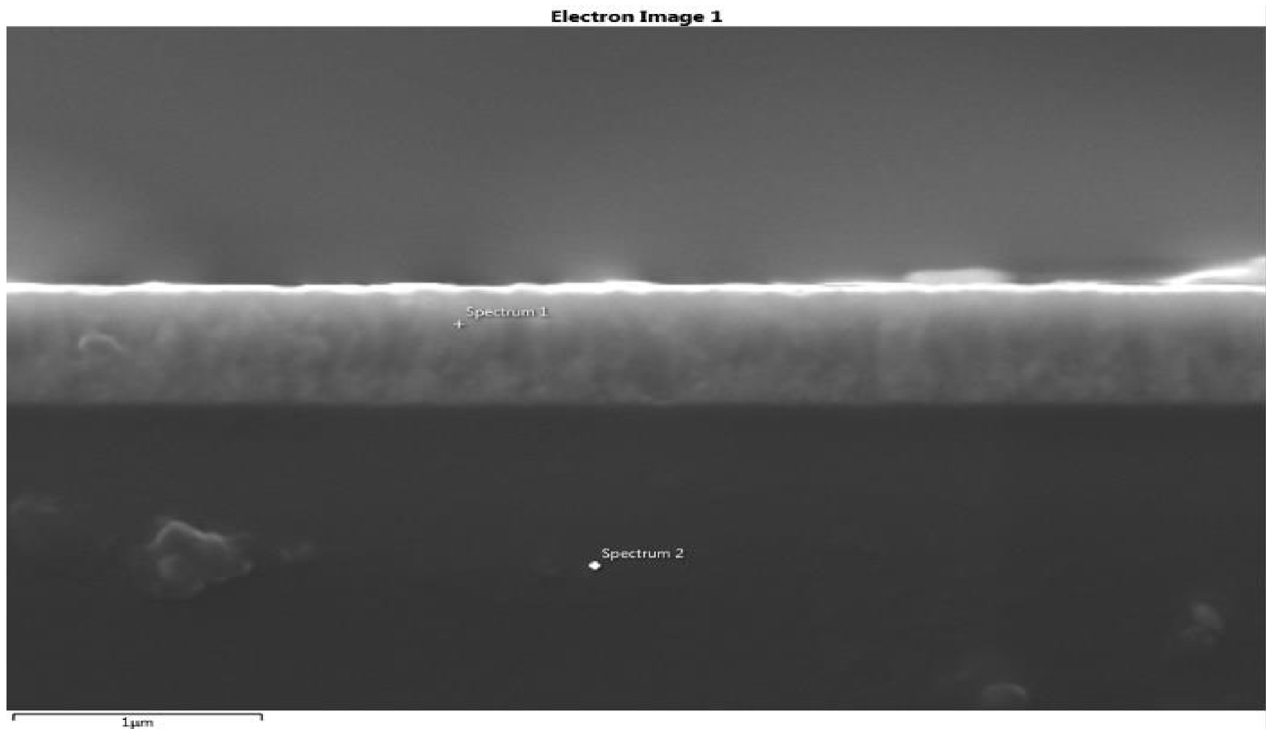

Figure 31: Cross sectional view of SEM result of sample 5

Figure 32: Cross sectional view of SEM result of sample 5 with film thickness measurement

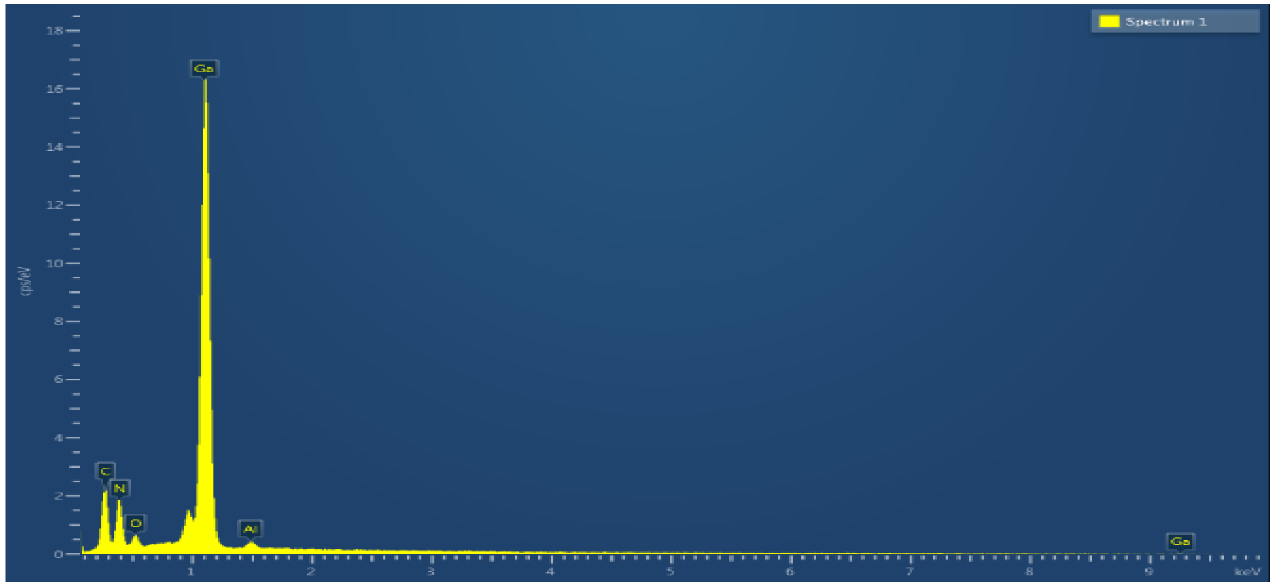

Figure 33: EDX result of sample 5 spectrum 1

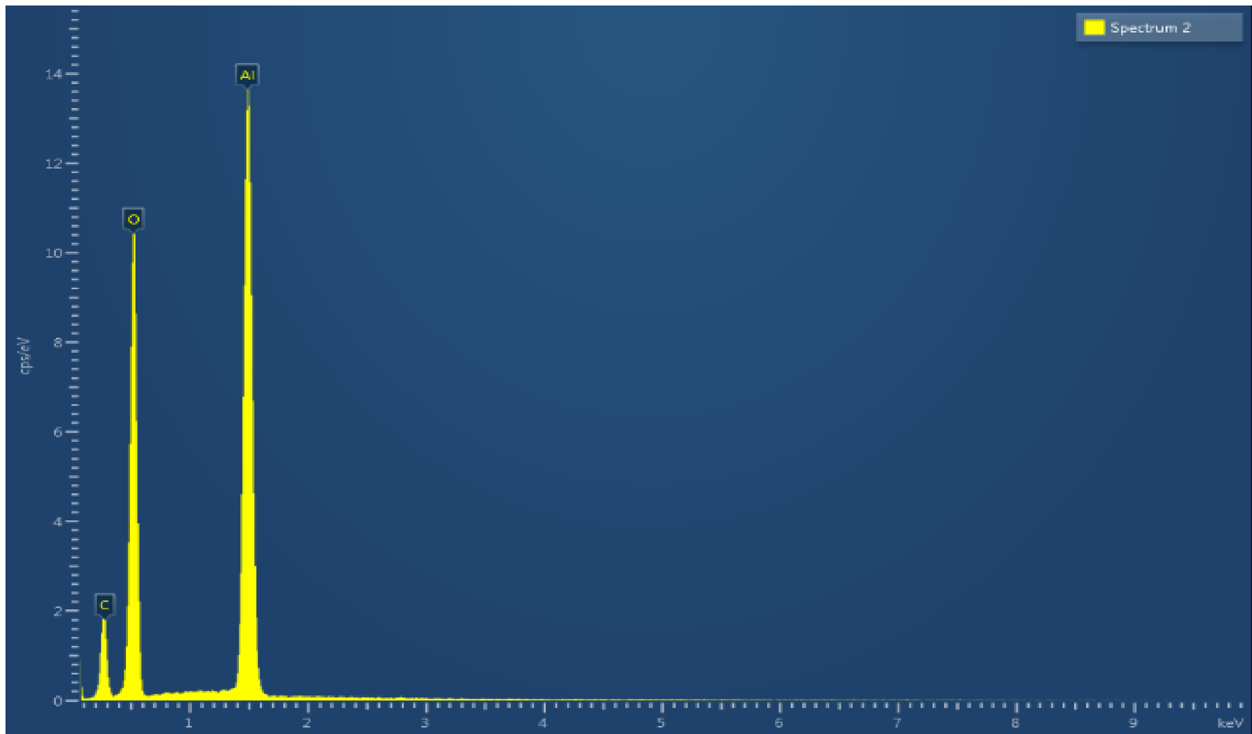

Figure 34: EDX result of sample 5 spectrum 2

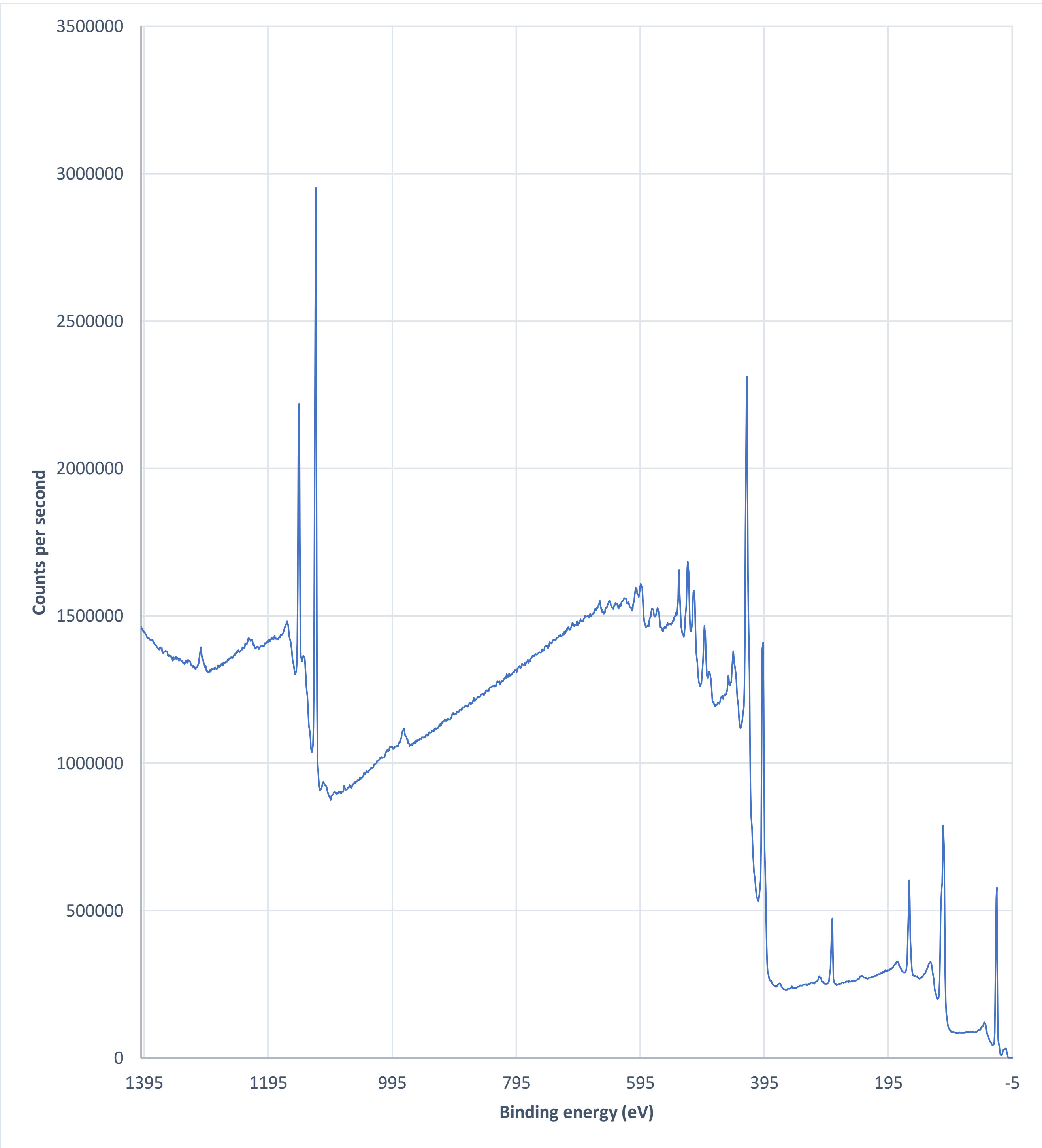

Figure 35: XPS result of sample 8

From the above growth result it is clear that obtaining p-doped GaN is difficult. To over come this difficulties post growth treatment can be done to activate Mg doped GaN films. Low energy electron beam irradiation LEEBI[108,109], thermal annealing[110, 111] and microwave treatment is used to achieve highly conductive Mg-doped GaN. Akasaki *et al.*3 used LEEBI to activate compensated Mg-doped GaN. However, a depth of 0.5mm was reached with acceleration voltage of 5-15 KV. Concludes LEEBI is not best method to be use to activate Mg in GaN thick resistive film. Nakamura *et al.*5 conducted thermal annealing on Mg doped GaN in order to reduce the resistivity. Annealing is conducted at 600-1200°C in nitrogen atmosphere. Thermal dissociation of GaN take place at high temperature due to dissociation pressure increase gradually at temperature above 700°C. Microwave treatment can be used to activate Mg at low temperature also with short time cycle. 2.45GHz, 560W microwave at different processing time is used to activate acceptor in Mg doped GaN. Along with microwave treatment, thermal annealing treatment is performed at 730°C for 20 minutes for comparison. The obtained result is analysed through hall effect and photoluminescence. Figure 36 shows photoluminescence spectra (a) 5 minutes microwave treatment, (b) 730°C, 20 minutes thermal annealing treatment (c) growth without any treatment. We have 437.5 nm blue peak with microwave treatment and thermal annealing when compared with as grown GaN. Figure 37, 38 shows hall effect measurement with resistivity and hole concentration of Mg doped

GaN layer performed at different amount of microwave treatment time. The measured resistivity is 1.1-1.65Ωcm[112] with hole concentration of 9.75×10^{17} cm^{-3}-2.15×10^{18} cm^{-3} [112]for microwave treatment with independent treatment time. The resistivity and hole concentration of 730°C 20 minutes thermal annealing treatment is 3.2Ωcm [112] and 6.58×10^{17} cm^{-3}[112]. Thus we can say Mg activation with microwave treatment is more effective than thermal annealing process. The main reason for Mg compensation in GaN film is due to hydrogen. With microwave treatment breaking of magnesium bond with hydrogen occur by the absorption of microwave energy. Microwave treatment is a very fast process as the resistivity and hole concentration are independent of treatment time.

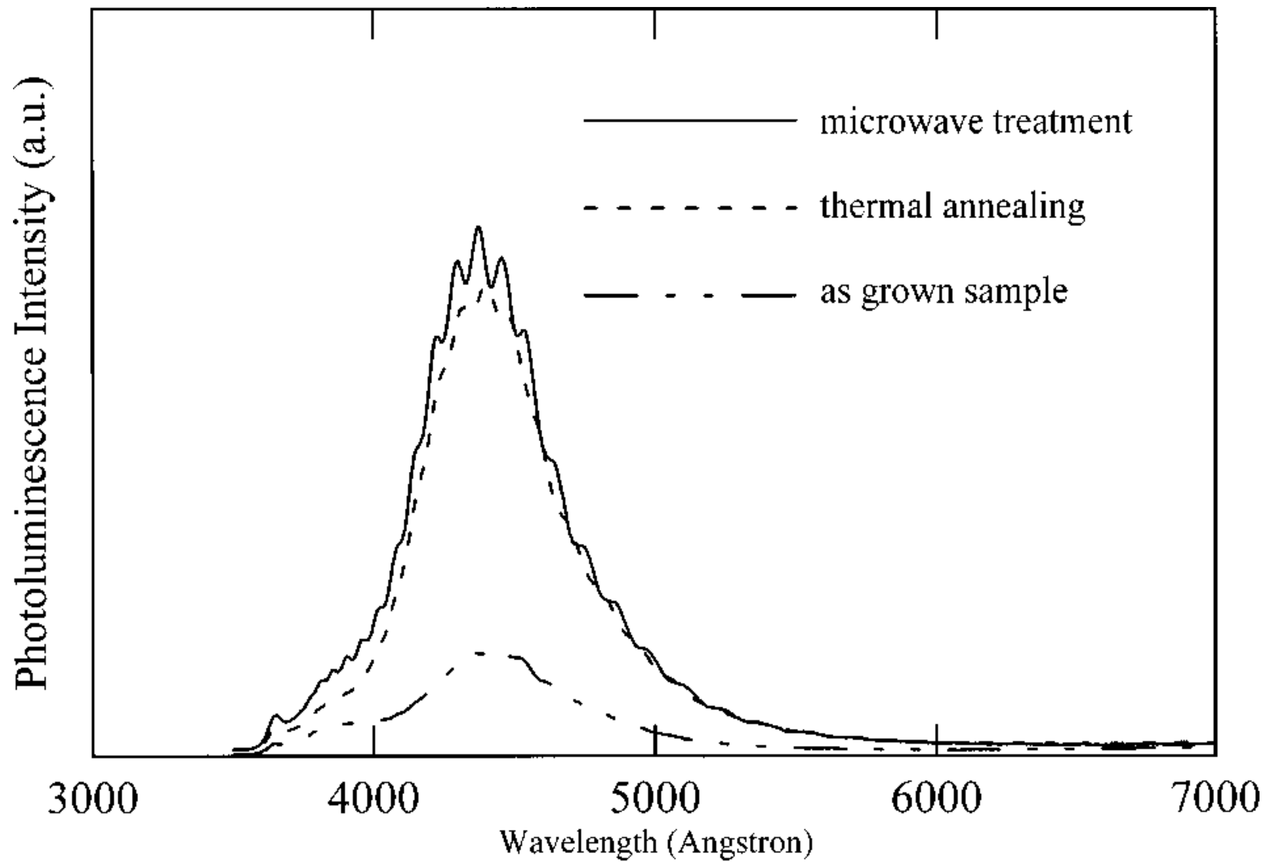

Figure 36: The photoluminescence spectra of Mg-doped GaN (a) with microwave treatment (b) with thermal annealing (c) as grown without any treatment.

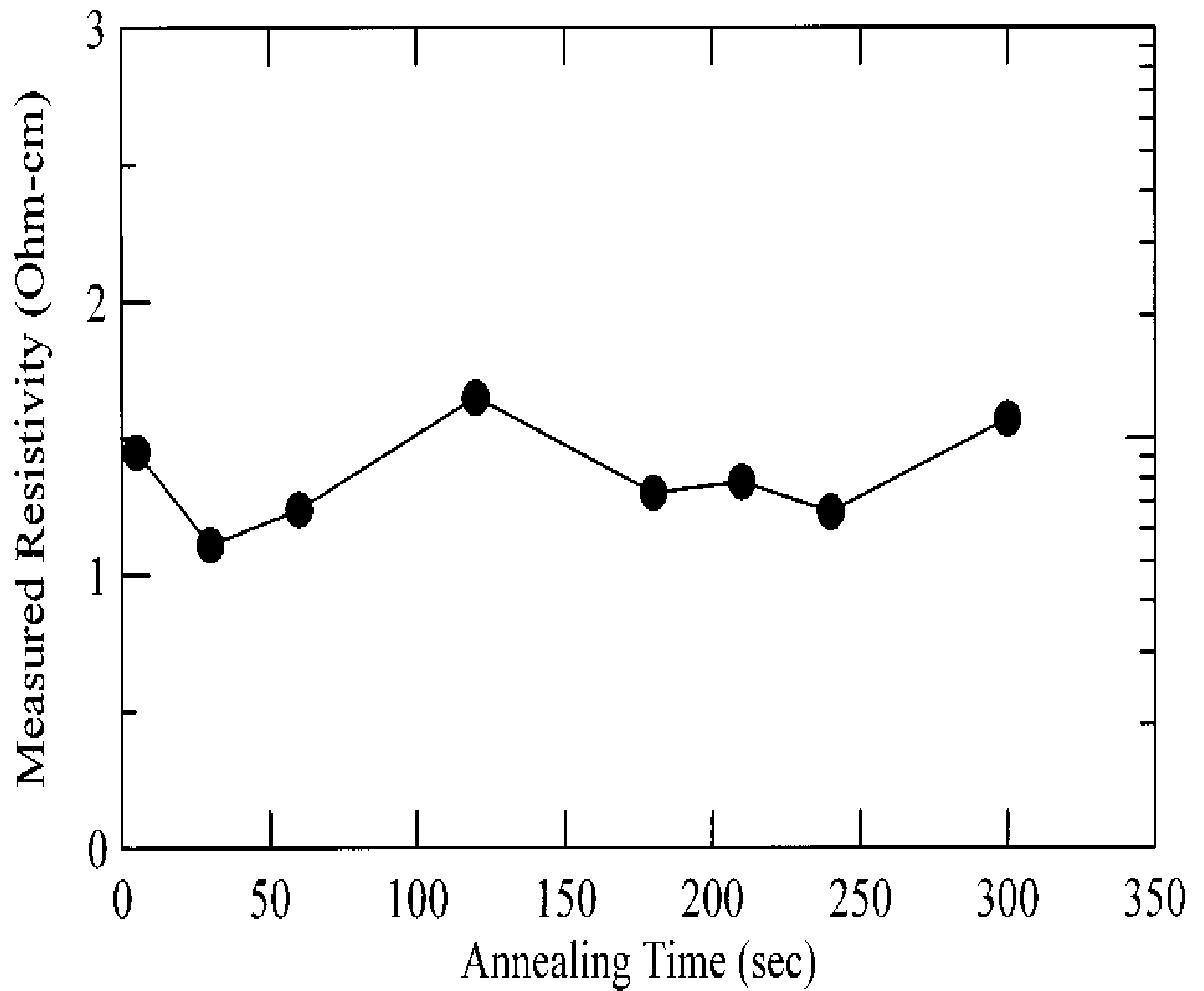

Figure 37: Resistivity of Mg-doped GaN with different microwave treatment time [112].

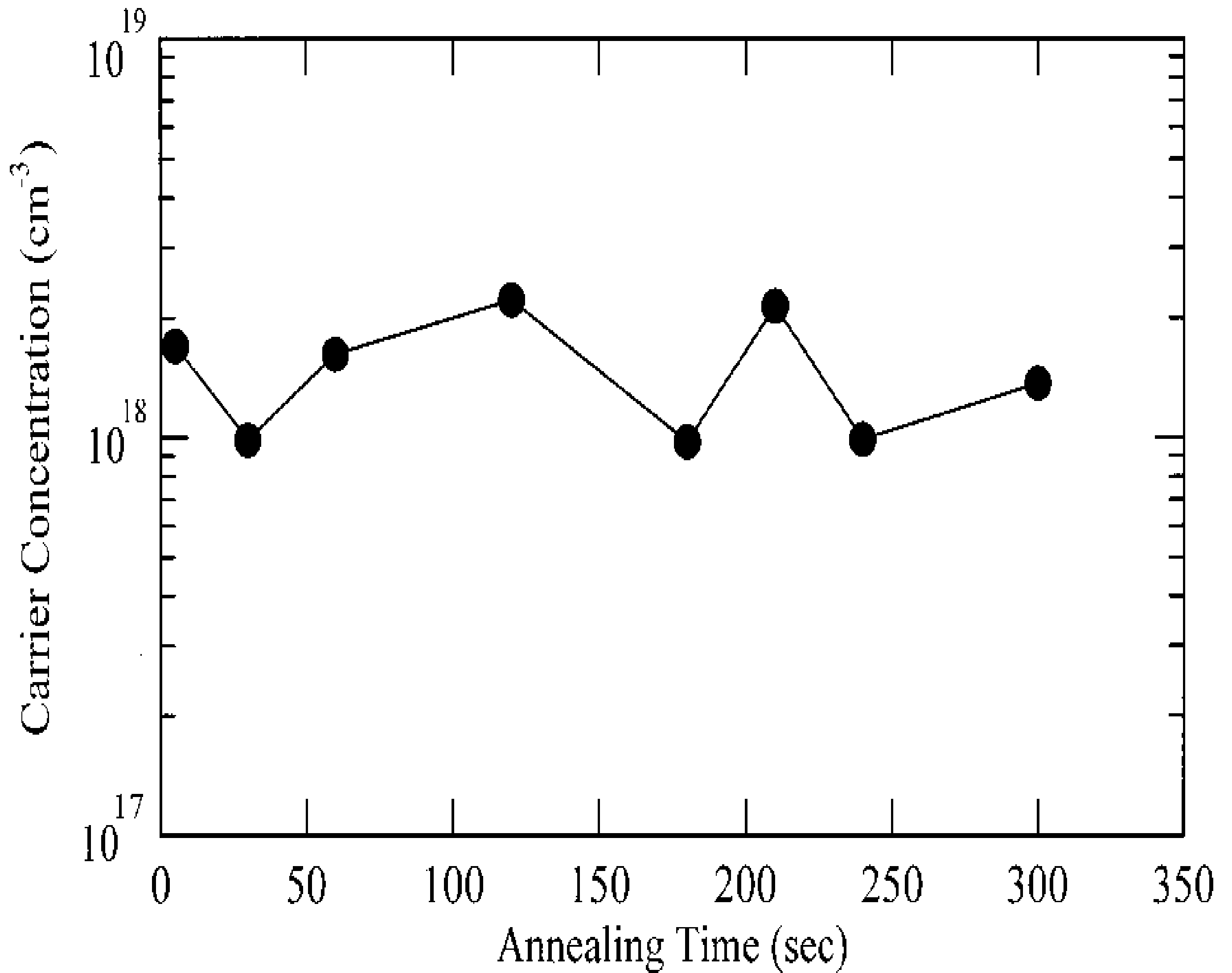

Figure 38: The carrier concentration of Mg-doped GaN by Hall measurement with different microwave treatment time[112].

Chapter 7: Conclusions

Growth of III-V nitride semiconductor using remote plasma metal organic chemical vapour deposition has been analyse and demonstrated. Sapphire is used as a substrate for the growth and Mg precursor for p-type doping. The reasons for limited doping are explained.

The obtained growth films are analysed through XRD, SEM and XPS. Result show GaN peak In XRD, presence of Mg is indicated my XPS, GaN thickness is shown in SEM.

Reference

1. H. Amano, I. Akasaki, T. Kozawa, K. Hiramatsu, N. Sawak, K. Ikeda, and Y. Ishi, J. Lumin. 40&41, 121 (1988).

2. P. Kozodoy, H. Xing, S. P. DenBaars, U. K. Mishra, A. Saxler, R. Perrin, S. Elhamri, and W. C. Mitchel, J. Appl. Phys. 87, 1832 (2000).

3. H. P. Maruska, J. J. Tietjen, and Appl. Phys. Lett. 15, 327 (1969).

4. E. Ejder and P. O. Fagerstrom, J. Phys. Chem. Solids 36, 289 (1975).

5. T. Kawabata, T. Matsuda, and S. Koike, J. Appl. Phys. 56, 2367 (1984).

6. P. Bergman, G. Ying, B. Monemar, and P. O. Holtz, J. Appl. Phys. 61, 4589 (1987).

7. C. H. Seager, A. F. Wright, J. Yu, and W. Gotz, J. Appl. Phys. 92, 6553 (2002).

8. H. Amano, M. Kito, K. Hiramtsu, and I. Akasaki, Jpn. J. Appl. Phys. 28, L2112 (1989).

9. S. Nakamura, T. Mukai, M. Senoh, and N. Isawa, Jpn. J. Appl. Phys. 31, L139 (1992).

10. J. C. Zolper, R. G. Wilson, S. J. Pearton, and R. A. Stall, Appl. Phys. Lett. 68, 1945 (1996).

11. S. Strite, Jpn. J. Appl. Phys. 33, L699 (1994).

12. M. A. Sanchez-Garcia, E. Calleja, F. J. Sanchez, F. Calle, E. Monroy, D. Basak, E.Munoz, C. Villar, A. Sanz-Hervas, M. Aguilar, J. J. Serizan, and J. M. Blanco, J. Elec. Mat. 27, 276 (1998).

13. D. J. Dewsnip, A. V. Andrianov, I. Harrison, J. W. Orton, D. E. Lacklison, G. B. Ren, S. E. Hooper, T. S. Cheng, and C. T. Foxon, Semicond. Sci. Technol. 13, 500 (1998).

14. H. Morkoç, *Handbook of Nitride Semiconductors and Devices, Materials Properties, Physics and Growth*. John Wiley & Sons, 2009.

15. G.B.Stringfellow, in *Organometallic Vapor-Phase Epitaxy: Theory and Practice*(Academic, Boston,1989)

16. D. J. Dewsnip, A. V. Andrianov, I. Harrison, J. W. Orton, D. E. Lacklison, G. B.Ren, S. E. Hooper, T. S. Cheng, and C. T. Foxon, Semicond. Sci. Technol. 13, 500 (1998).

17. T. D. Moustakas and R. J. Molnar, Mater. Res. Soc. Symp. Proc. 281, 753 (1993).

18. J. Ptak, Ph. D. Dissertation Thesis, West Virginia University, 2001.

19. T. H. Myers, L. S. Hirsch, L. T. Romano, and M. R. Richards-Babb, J. Vac. Sci. Technol. B 16, 2261 (1998).

20. J. M. Myoung and K. Kim, J. of Vac. Sci. Technol. A 18, 450 (2000).

21. J. M. Myoung, K. H. Shim, O. Gluschenkov, C. Kim, K. Kim, S. Kim, and S. G. Bishop, J. Crys. Grow. 182, 241 (1997).

22. U. Kaufmann, P. Schlotter, H. Obloh, K. Kohler, and M. Maier, Phys. Rev. B 62, 10867 (2000).

23. J. M. Myoung and K. Kim, J. of Vac. Sci. Technol. A 18, 450 (2000).

24. U. Kaufmann, P. Schlotter, H. Obloh, K. Kohler, and M. Maier, Phys. Rev. B 62, 10867 (2000).

25. Q. Sun, A. Selloni, T. H. Myers, and W. A. Doolittle, Phys. Rev. B 73, 155337 (2006).

26. Z. Liliental-Weber, M. Benamara, J. Washburn, I. Grzegory, S. Porowski, D. J. H. Lambert, C. J. Eiting, and R. D. Dupuis, Appl. Phys. Lett. 75, 4159 (1999).

27. P. Vennegues, M. Leroux, S. Dalmasso, M. Benaissa, P. D. Mierry, P. Lorenzini, B. Damilano, B. Beaumont, J. Massies, and P. Gibart, Phys. Rev. B 68, 235214 (2003).J. Ptak, T. H. Myers, L. T. Romano, C. G. V. d. Walle, and J. E. Northrup, Appl. Phys. Lett. 78, 285 (2001).

28. Z. Liliental-Weber, T. Tomaszewicz, D. Zakharov, J. Jasinski, and M. A. OKeefe, Phys. Rev. Lett. 93, 206102 (2004).

29. J. M. Myoung and K. Kim, J. of Vac. Sci. Technol. A 18, 450 (2000).

30. P. Vennegues, M. Leroux, S. Dalmasso, M. Benaissa, P. D. Mierry, P. Lorenzini, B. Damilano, B. Beaumont, J. Massies, and P. Gibart, Phys. Rev. B 68, 235214 (2003).

31. Y. Sun, L. S. Tan, S. J. Chua, and S. Prakash, Mat. Res. Soc. Symp. 595, W3.82.1 - W3.82.7 (2000).

32. K. H. Ploog and O. Brandt, Vac. Sci. Technol. A 16, 1609 (1998).

33. C. G. V. d. Walle, S. Limpijumnong, and J. Neugebauer, Phys. Rev. B 63, 245205 (2001).

34. Keun-Man Song, Dong-Joon Kim, Yong-Tae Moon, Seong-Ju Park Journal of Crystal Growth 233 (2001) 439–445

35. T.F. Kuech, R. Potemski, F. Cardone, J. Crystal Growth 124 (1992) 318.

36. M.S. Goorsky, T.F. Kuech, R.M. Potemski, J. Electrochem. Soc. 138 (1991) 1817. Narmann, M.L. Yu, Surf. Sci. 270 (1992) 1041.

37. L. Zhang, S.L. Gu, T.F. Kuech, Marek P. Boleslawski, J.Crystal Growth 213 (2000) 1}9.

38. B. Beaumont, P. Gibart, J. P. Faurie, J. Cryst. Growth 156, 140 (1995).

39. B. Beaumont, M. Vaille, P. Lorenzini, Pierre Gibart, T. Boufaden, B. el Jani, *Alternative N*

40. *precursors and Mg doped GaN grown by MOVPE,* MRS Internet J. Nitride Semicond. Res. 1,17(1996).

41. C-H. Hong, D. Pavlidis, K. Hong, K. Wang and J. Singh, *GaN and AlN OMVPE GrowthUsing Phenylhydrazine*, 1993 International Conference on Silicon Carbide and Related Materials, Washington D.C., November 1993, Institute of Physics Conference Series, No.137, Chapter 4, pp. 413-415.

42. S.Yoshida, J.Suzuki, J.Crystal Growth, 191 1-2 (1998) 279-281

43. Zhi-Jie Liu, Burak Atakan, Katharina Kohse-Hoinghaus, Journal of Crystal Growth 219(2000) 176-179

44. S. Nakamura, M. Senoh, T. Mukai, Jpn. J. Appl. Phys. 30, L1708 (1991).

45. [66]W. Goetz, R. S. Kern, C. H. Chen, H. Liu, D. A. Steigerwald, R. M. Fletcher, Mater. Sci.Eng. B 59, 211 (1999).

46. Y.Ohuchi, K.Tadatomo, H.Nakayama, N.Kaneda, T.Detchprohm, K.Hiramatsu, N.Sawaki,
47. J.Crystal Growth 170 (1997) 325-328

48. B. Beaumont, S. Haffouz, P. Gibart,, M. Leroux , Ph. Lorenzini, E. Calleja, E. Munoz, Materials Science and Engineering B50 (1997) 296–301

49. B. Beaumont, M. Vaille, P. Lorenzini, Pierre Gibart, T. Boufaden, B. el Jani, *Alternative N*
50. *precursors and Mg doped GaN grown by MOVPE,* MRS Internet J. Nitride Semicond. Res. 1,
51. 17(1996).

52. P. de Mierry, B. Beaumont, E. Feltin, H.P.D. Schenk, Pierre Gibart, F. Jomard, S. Rushworth,
53. L. Smith, R. Odedra, MRS Internet J. Nitride Semicond. Res. 5, 8(2000).

54. S.Nakamura, T.Mukai, M.Senoh, and N.Iwasa, Jpn. J. Appl. Phys. 31, L139 (1992)

55. H.Amano, M.Kito, K.Hiramatsu, and I.Akasaki, Jpn. J. Appl. Phys. 28, L2112(1989)

56. I.Akasaki, H.Zmano, M.Kito and K.Hiramatsu, J.Lumin. 48&49 (1991) 666

57. K. S. Kim, C. S. Oh, J.-H. Kim, K. J. Lee, G. M. Yang, J. W. Yang, C.-H. Hong, K. Y. Lim,
58. and H. J. Lee, MRS Internet J. Nitride Semicond. Res. 5S1, W3.84 (2000).

59. H. Amano, N. Sawaki, I. Akasaki, and Y. Toyoda, "Metalorganic vapor phase epitaxial growth of a high quality GaN film using an AlN buffer layer," *Appl. Phys. Lett.*, vol. 48, no. 5, pp. 353–355, Feb. 1986.

60. S. Nakamura, M. Senoh, and T. Mukai, "Highly P-Typed Mg-Doped GaN Films Grown with GaN Buffer Layers," *Jpn. J. Appl. Phys.*, vol. 30, no. Part 2, No. 10A, pp. L1708–L1711, Oct.

61. Q. Sun and J. Han, "Nonpolar and semipolar GaN heteroepitaxy on sapphire for LED application," 2010, vol. 7617, pp. 761717–761717–14.

62. M. Yang, B. Yao, Y. H. Sohn, and R. D. Sisson, “Simulation of the ferritic nitriding process,” *Int. Heat Treat. Surf. Eng.*, vol. 5, no. 3, pp. 122–126, 2011.

63. J.-S. Paek, K.-K. Kim, J.-M. Lee, D.-J. Kim, M.-S. Yi, D. Y. Noh, H.-G. Kim, and S.-J. Park, “Nitridation of sapphire substrate and its effect on the growth of GaN layer at low temperature,” *J. Cryst. Growth*, vol. 200, no. 1–2, pp. 55–62, Apr. 1999.

64. Y. Tsukada, Y. Enatsu, S. Kubo, H. Ikeda, K. Kurihara, H. Matsumoto, S. Nagao, Y. Mikawa, and K. Fujito, “High-quality, 2-inch-diameter *m* -plane GaN substrates grown by hydride vapor phase epitaxy on acidic ammonothermal seeds,” *Jpn. J. Appl. Phys.*, vol. 55, no. 5S, p. 05FC01, May 2016. Rockett, *The Materials Science of Semiconductors*. Springer, 2008.

65. G. B. Stringfellow, “Microstructures produced during the epitaxial growth of InGaN alloys,” *J. Cryst. Growth*, vol. 312, no. 6, pp. 735–749, Mar. 2010.

66. N. P, *English: Concept Drawing of a Molecular Beam Epitaxy Growth chamber*. 2013.

67. H. B. Profijt, S. E. Potts, M. C. M. Van de Sanden, and W. M. M. Kessels, “Plasma-assisted atomic layer deposition: Basics, opportunities, and challenges,” *J. Vac. Sci. Technol. A*, vol. 29, no. 5, p. 050801, 2011.

68. T. Nagata, M. Haemori, Y. Sakuma, T. Chikyow, J. Anzai, and T. Uehara, “Hydrogen effect on near-atmospheric nitrogen plasma assisted chemical vapor deposition of GaN film growth,” *J. Appl. Phys.*, vol. 105, no. 6, pp. 066106–066109, Mar. 2009.

69. E. Iliopoulos, A. Adikimenakis, E. Dimakis, K. Tsagaraki, G. Konstantinidis, and A. Georgakilas, “Active nitrogen species dependence on radiofrequency plasma source operating parameters and their role in GaN growth,” *J. Cryst. Growth*, vol. 278, no. 1–4, pp. 426–430, May 2005.

70. Y.-S. Tang, S.-F. Hu, C. C. Lin, N. C. Bagkar, and R.-S. Liu, “Thermally stable luminescence of KSrPO4:Eu2+ phosphor for white light UV light-emitting diodes,” *Appl. Phys. Lett.*, vol. 90, no. 15, p. 151108, Apr. 2007.

71. Low temperature epitaxial growths of III-nitride semiconductors on ITO glass substrate.

72. F. Lecourt *et al.*, “InAlN/GaN HEMTs on Sapphire Substrate With 2.9-W/mm Output Power Density at 18 GHz,” *IEEE Electron Device Lett.*, vol. 32, no. 11, pp. 1537–1539, Nov. 2011.

73. Q. Xia, H. Xia, and A. L. Ruoff, “Pressure-induced rocksalt phase of aluminum nitride: A metastable structure at ambient condition,” *J. Appl. Phys.*, vol. 73, no. 12, pp. 8198–8200, Jun. 1993.

74. N. Koide, H. Kato, M. Sassa, S. Yamasaki, K. Manabe, M. Hashimoto, H. Amano, K.Hiramatsu, and I. Akasaki, "Doping of Gan with Si and Properties of Blue

M/I/N/N+ Gan Led with Si-Doped N+-Layer by Movpe," *Journal of Crystal Growth,* vol. 115, pp. 639-642, Dec 1991.

75. W. Gotz, R. S. Kern, C. H. Chen, H. Liu, D. A. Steigerwald, and R. M. Fletcher, "Hall-effect characterization of III-V nitride semiconductors for high efficiency light emitting diodes," *Materials Science and Engineering B-Solid State Materials for Advanced Technology,* vol. 59, pp. 211-217, May 1999.

76. J. B. Webb, H. Tang, S. Rolfe, and J. A. Bardwell, "Semi-insulating C-doped GaN and high-mobility AlGaN/GaN heterostructures grown by ammonia molecular beam epitaxy," *Applied Physics Letters,* vol. 75, pp. 953-955, Aug 1999.

77. H. Amano, I. Akasaki, T. Kozawa, K. Hiramatsu, N. Sawaki, K. Ikeda, and Y. Ishii, "Electron-Beam Effects on Blue Luminescence of Zinc-Doped Gan," *Journal of Luminescence,* vol. 40-1, pp. 121-122, Feb 1988.

78. L. Pauling, "The Properties of Solutions," in *General Chemistry* New York: Dover Publications, 1970, pp. 447-480.

79. P. Vennegues, M. Leroux, S. Dalmasso, M. Benaissa, P. De Mierry, P. Lorenzini, B. Damilano, B. Beaumont, J. Massies, and P. Gibart, "Atomic structure of pyramidal defects in Mg-doped GaN," *Physical Review B,* vol. 68, Dec 2003.

80. J. P. Schaffer, A. Saxena, S. D. Antolovich, T. H. Sanders, Jr., and S. B. Warner, "Crystal Structures," in *The Science and Design of Engineering Materials* Boston: McGraw-Hill, 1999, pp. 60-109.

81. J. Neugebauer and C. G. Van de Walle, "Theory of point defects and complexes in GaN," *Materials Research Society Symposium - Proceedings,* vol. 395, pp. 645-656, 1996.

82. Q. A. Sun, A. Selloni, T. H. Myers, and W. A. Doolittle, "Energetics of Mg incorporation at GaN(0001) and GaN(0001) surfaces," *Physical Review B,* vol. 73, Apr 2006.

83. S. Figge, R. Kroger, T. Bottcher, P. L. Ryder, and D. Hommel, "Magnesium segregation and the formation of pyramidal defects in p-GaN," *Applied Physics Letters,* vol. 81, pp. 4748-4750, Dec 2002.

84. V. Ramachandran, R. M. Feenstra, W. L. Sarney, L. Salamanca-Riba, J. E. Northrup, L. T. Romano, and D. W. Greve, "Inversion of wurtzite GaN(0001) by exposure to magnesium," *Applied Physics Letters,* vol. 75, pp. 808-810, Aug 1999.

85. B. Beaumont, S. Haffouz, and P. Gibart, "Magnesium induced changes in the selective growth of GaN by metalorganic vapor phase epitaxy," *Applied Physics Letters,* vol. 72, pp. 921-923, Feb 1998.

86. Z. Liliental-Weber, M. Benamara, W. Swider, J. Washburn, I. Grzegory, S. Porowski, D. J. H. Lambert, C. J. Eiting, and R. D. Dupuis, "Mg-doped GaN: Similar defects in bulk crystals and layers grown on Al2O3 by metal-organic chemical-vapor deposition," *Applied Physics Letters,* vol. 75, pp. 4159-4161, Dec 1999.

87. P. Vennegues, M. Benaissa, B. Beaumont, E. Feltin, P. De Mierry, S. Dalmasso, M. Leroux, and P. Gibart, "Pyramidal defects in metalorganic vapor phase.

88. B. Y. Ber, Y. A. Kudriavtsev, A. V. Merkulov, S. V. Novikov, D. E. Lacklison, J. W. Orton, T. S. Cheng, and C. T. Foxton, "Secondary ion mass spectroscopy investigations of magnesium and carbon doped gallium nitride films grown by molecular beam epitaxy," *Semiconductor Science and Technology,* vol. 13, pp.71-74, Jan 1998.

89. M. L. Timmons, P. K. Chiang, and S. V. Hattangady, "An alternative Mg precursor for p-type doping of OMVPE grown material," *Journal of Crystal Growth,* vol. 77, pp. 37-41, 1986.

90. G. Namkoong, W. A. Doolittle, and A. S. Brown, "Incorporation of Mg in GaN grown by plasma-assisted molecular beam epitaxy," *Applied Physics Letters,* vol. 77, pp. 4386-4388, December 25 2000.

91. Veeco, "Vapor Pressure Data For Selected Elements," http://www.veeco.com/library/elements/images/VaporPress2b_large.jpg, 2006.

92. H. Luth, "Preparation of Well-Defined Surfaces, Interfaces and Thin Films," in *Solid Surfaces, Interfaces and Thin Films* New York: Springer, 2001, pp. 33-76.

93. M. Ohring, "Thin-Film Evaporation Process," in *Materials Science of Thin Films*, 2nd ed San Diego: Academic Press, 2002, pp. 95-144.

94. Veeco, "Crucible dimensions of a high temperature source," St. Paul: http://www.veeco.com/pdfs.php/220, 2005.

95. B. Y. Ber, Y. A. Kudriavtsev, A. V. Merkulov, S. V. Novikov, D. E. Lacklison, J. W. Orton, T. S. Cheng, and C. T. Foxon, "Secondary ion mass spectroscopy investigations of magnesium and carbon doped gallium nitride films grown by molecular beam epitaxy," *Semiconductor Science and Technology,* vol. 13, pp. 71-74, Jan 1998. S. Barker and M. Ilegems, "Infrared Lattice-Vibrations and Free-Electron Dispersion in Gan," *Physical Review B,* vol. 7, pp. 743-750, 1973.

96. M. Shur, *GaAs Devices and Circuits*. New York: Plenum Press, 1987.

97. G. D. Chen, M. Smith, J. Y. Lin, H. X. Jiang, S. H. Wei, M. A. Khan, and C. J. Sun, "Fundamental optical transitions in GaN," *Applied Physics Letters,* vol. 68, pp. 2784-2786, May 1996.

98. P. Kozodoy, H. L. Xing, S. P. DenBaars, U. K. Mishra, A. Saxler, R. Perrin, S. Elhamri, and W. C. Mitchel, "Heavy doping effects in Mg-doped GaN," *Journal of Applied Physics,* vol. 87, pp. 1832-1835, Feb 2000.

99. H. Nakayama, P. Hacke, M. R. H. Khan, T. Detchprohm, K. Hiramatsu, and N. Sawaki, "Electrical transport properties of p-GaN," *Japanese Journal of Applied Physics Part 2-Letters,* vol. 35, pp. L282-L284, Mar 1996.

100. T. Tanaka, A. Watanabe, H. Amano, Y. Kobayashi, I. Akasaki, S. Yamazaki, and M. Koike, "P-Type Conduction in Mg-Doped Gan and Al0.08ga0.92n Grown by Metalorganic Vapor-Phase Epitaxy," *Applied Physics Letters,* vol. 65, pp. 593- 594, Aug 1994.

101. D. Huang, F. Yun, M. A. Reshchikov, D. Wang, H. Morkoc, D. L. Rode, L. A. Farina, C. Kurdak, K. T. Tsen, S. S. Park, and K. Y. Lee, "Hall mobility and carrier concentration in free-standing high quality GaN templates grown by hydride vapor phase epitaxy," *Solid-State Electronics,* vol. 45, pp. 711-715, May 2001.

102. S. Nakamura, M. Senoh, and T. Mukai, "Highly P-Typed Mg-Doped Gan Films Grown with Gan Buffer Layers," *Japanese Journal of Applied Physics Part 2-Letters,* vol. 30, pp. L1708-L1711, Oct 1991.

103. D. W. Covington and E. L. Meeks, "Unintentional dopants incorporated in GaAs layers grown by molecular beam epitaxy," *Journal of Vacuum Science & Technology,* vol. 16, pp. 847-850, 1979.

104. J. Neugebauer and C. G. Vandewalle, "Hydrogen in Gan - Novel Aspects of a Common Impurity," *Physical Review Letters,* vol. 75, pp. 4452-4455, Dec 1995.

105. S. Nakamura, T. Mukai, M. Senoh, and N. Iwasa, "Thermal Annealing Effects on P-Type Mg-Doped GaN Films," *Japan Journal of Applied Physics,* vol. 31, pp. L139-L142, 15 February 1992.

106. Journal of Microwaves and Optoelectronics, Vol. 2, N.o 5, July 2002.

107. Gallium Nitride, Indium Nitride, and Heterostructure Development Using The MEAglow Growth System.

108. W. Gotz, N. M. Johnson, J. Walker, D. P. Bour, and R. A. Street, Appl. Phys. Lett. **67**, 2666 ~1995.

109. S. Nakamura, N. Iwasa, M. Senoh, and T. Mukai, Jpn. J. Appl. Phys., Part **31**, 1258 ~1992.

110. H. Amano, M. Kito, K. Hiramatsu, and I. Akasaki, Jpn. J. Appl. Phys., Part 2 **28**, L2112 ~1989.

111. H. Amano, I. Akasaki, T. Kozawa, K. Hiramatsu, N. Sawaki, K. Ikeda,and Y. Ishii, J. Lumin. **40&41**, 121 ~1988.

112. Appl. Phys. Lett. **78**, 312 (2001); doi: 10.1063/1.1340864